

St. John's University

St. John's Scholar

---

Theses and Dissertations

---

2021

## STRUCTURE BASED OPTIMIZATION OF BENZIMIDAZOLE 4-CARBOXAMIDE SCAFFOLD LED TO PICOMOLAR POLY(ADP- RIBOSE) POLYMERASE INHIBITORS

Griffin J. Coate

*Saint John's University, Jamaica New York*

Follow this and additional works at: [https://scholar.stjohns.edu/theses\\_dissertations](https://scholar.stjohns.edu/theses_dissertations)



Part of the [Pharmacy and Pharmaceutical Sciences Commons](#)

---

### Recommended Citation

Coate, Griffin J., "STRUCTURE BASED OPTIMIZATION OF BENZIMIDAZOLE 4-CARBOXAMIDE SCAFFOLD LED TO PICOMOLAR POLY(ADP-RIBOSE) POLYMERASE INHIBITORS" (2021). *Theses and Dissertations*. 302.

[https://scholar.stjohns.edu/theses\\_dissertations/302](https://scholar.stjohns.edu/theses_dissertations/302)

This Thesis is brought to you for free and open access by St. John's Scholar. It has been accepted for inclusion in Theses and Dissertations by an authorized administrator of St. John's Scholar. For more information, please contact [karniks@stjohns.edu](mailto:karniks@stjohns.edu), [fuchsc@stjohns.edu](mailto:fuchsc@stjohns.edu).

STRUCTURE BASED OPTIMIZATION OF BENZIMIDAZOLE 4-CARBOXAMIDE  
SCAFFOLD LED TO PICOMOLAR POLY(ADP-RIBOSE) POLYMERASE  
INHIBITORS

A thesis submitted in partial fulfillment  
of the requirements for the degree of

MASTER OF SCIENCE

to the faculty of the

DEPARTMENT OF PHARMACEUTICAL SCIENCES  
of

COLLEGE OF PHARMACY AND HEALTH SCIENCES

at

ST. JOHN'S UNIVERSITY

New York

by

GRIFFIN COATE

Date Submitted 5/31/2021

Date Approved 6/25/2021

---

---

Griffin Coate

Dr. Tanaji Talele

**© Copyright by Griffin Coate 2021**

**All Rights Reserved**

## ABSTRACT

### STRUCTURE BASED OPTIMIZATION OF BENZIMIDAZOLE 4-CARBOXAMIDE SCAFFOLD LED TO PICOMOLAR POLY(ADP-RIBOSE) POLYMERASE INHIBITORS

Griffin Coate

Poly(ADP-ribose) polymerase 1 (PARP1) is one of several proteins in the PARP superfamily consisting of 17 proteins with a conserved ART domain. Out of the 17 total proteins, 6 show clear evidence of catalytic activity. These 6 proteins are comprised of PARP1 through PARP4 as well as TNKS1 and TNKS2. PARP1 is thoroughly characterized and has been implicated for its role in various forms of cancer. Due to the role PARP1 plays in the DNA repair pathway, targeting PARP1 for inhibition has led to two distinct anticancer strategies. The first focusing on combinatorial drug therapy with a DNA damaging anticancer agent. DNA-damaging anticancer treatments lead to overactivation of DNA repair pathways, which PARP1 is heavily involved in. This can lead to drug resistance, unless PARP1 is adequately inhibited. The second strategy is the PARP1 inhibitor as a single agent treatment to be utilized in DNA repair deficient patients such as BRCA deficiency. Encouraged by the ability of benzimidazole-4-carboxamide-derived lead compound (1, UKTT-15, PARP1 IC<sub>50</sub> = 2.6 nM) to form a cytotoxic PARP1/DNA complex, a study was initiated to further improve its potency as a PARP1 inhibitor while also improving upon the sub-optimal chemical/metabolic stability. The current report features the efforts taken to achieve these goals, wherein we optimized 1 via four molecular modifications by: (1) replacing the methyl ester group with a wide

range of stable functional groups, (2) replacing the C6-H with a fluorine on the benzimidazole-4-carboxamide scaffold, (3) replacing the piperazine linker with aminomethylazetidione, and (4) testing salt intermediates without the pyrimidine ring. This led to a series of drug-like compounds (e.g., 2 – 23) with lead compounds exhibiting single digit nanomolar to picomolar potency against PARP1. Predicted binding models of target compounds using PARP1-1 co-crystal structure facilitated interpretation of observed structure-activity relationship data. In addition, representative set of compounds showed improved aqueous solubility and stability at pH4.0/7.4 compared to 1. Moreover, a clean selectivity profile of representative set of 6 compounds was observed when screened against kinases (Ser/Thr and tyrosine) at 100 nM.

## ACKNOWLEDGEMENT

First, I would like to extend my sincere gratitude to Dr. Tanaji Talele for the relentless encouragement, corrections, and guidance through every step of this process. Without Dr. Talele's expertise and the constant push to improve myself this would have been impossible. Next, I would like to thank the members of my defense committee Dr. Vijaya Korlipara and Dr. Carlos Sanhueza Chavez. I would like to extend my sincere gratitude towards Dr. Suman Pathi for using his expertise to guide and assist me in the lab. Next, I would like to thank my colleagues in the department of Medicinal Chemistry for accepting me as a member of the program and for their help along the way. To Dr. Woon-Kai Low, I would like to extend my sincere gratitude for encouraging me to pursue a thesis. Finally, thank you to the PHS department for providing the resources for my research.

I would also like to thank my parents; Marcy and Tom, as they have supported and encouraged me throughout my entire academic career, and this would not have been possible without them. I would also like to thank my siblings Ben and Cooper for their support.

## TABLE OF CONTENTS

Acknowledgments.....	ii
List of Tables.....	vi
List of Figures.....	vii
List of Schemes.....	viii
1. Introduction.....	1
2. Results and Discussion.....	4
2.1. Structure-Based Design of Highly Potent PARP1 Inhibitors Targeting ABP and $\alpha$ F-Helix.....	4
2.2. Structure-Activity Relationship.....	6
2.2.1. Optimization of ABP-Binding Pyrimidine Tail Motif to Introduce Steric Clashes with $\alpha$ F-Helix of HD.....	7
2.2.2. Investigation of the Fluorine Effect on Biochemical PARP1 Potency.....	9
2.2.3. Effect of replacing the Piperazine linker with aminomethylazetidine.....	11
2.2.4. Drug-like derivatives of BI-4-CONH <sub>2</sub> scaffold.....	12
2.3. In Vitro ADME Parameters of Selected Compounds (5, 6, 7, 9, 12, 14, 15, 17, 18, 19, 21, and 22).....	14
2.4. Binding Model for Key Compounds within the active site of PARP1.....	16
2.5. Specificities and Off-Targets within the PARP family.....	18
2.6. Kinase Panel Assay.....	19
3. Chemistry.....	21
4. Summary.....	29
5. Experimental.....	30
5.1. Chemical Synthesis.....	30
5.1.1. Preparation of 2-(4-(4-(5-Ethynylpyrimidin-2-yl)piperazine-1- carbonyl)phenyl)-1H-benzo[d]imidazole-4-carboxamide ( <b>2</b> ).....	32
5.1.2. 2-(4-(4-(5-(Azetidine-1-carbonyl)pyrimidin-2-yl)piperazine-1- carbonyl)phenyl)-1H-benzo- [d]imidazole-4-carboxamide ( <b>3</b> ).....	32
5.1.3. 2-(4-(4-(5-((2,2,2-trifluoroethyl)carbonyl)pyrimidin-2-yl)piperazine-1- carbonyl)phenyl) -1H-benzo[d]imidazole-4-carboxamide ( <b>4</b> ).....	33

5.1.4. 2-(4-(4-(5-(Cyclopropylcarbamoyl)pyrimidin-2-yl)piperazine-1-carbonyl)phenyl)-1H-benzo- [d]imidazole-4-carboxamide (5).....	34
5.1.5. 2-(4-(4-(5-(bicyclo[1.1.1]pentan-1-ylcarbamoyl)pyrimidin-2-yl)piperazine-1-carbonyl)- phenyl)-1H-benzo[d]imidazole-4-carboxamide (6).....	34
5.1.6. 2-(4-(4-(5-(oxetan-3-ylcarbamoyl)pyrimidin-2-yl)piperazine-1-carbonyl)phenyl)-1H-benzo- [d]imidazole-4-carboxamide (7).....	35
5.1.7. 2-(4-(4-(5-(oxetan-3-ylcarbamoyl)pyrimidin-2-yl)piperazine-1-carbonyl)phenyl)-1H-benzo- [d]imidazole-4-carboxamide (8).....	35
5.1.8. [4-(cyclopropylcarbamoyl)pyrimidin-2-yl]piperazine-1-carbonyl} phenyl)-1H-1,3-benzodiazole -4-carboxamide (9).....	36
5.1.9. 2-(4-(4-(5-(bicyclo[1.1.1]pentan-1-ylcarbamoyl)pyrimidin-2-yl)piperazine-1-carbonyl)- phenyl)-6-fluoro-1H-benzo[d]imidazole-4-carboxamide (10).....	36
5.1.10. 2-(4-(4-(4-(bicyclo[1.1.1]pentan-1-ylcarbamoyl)pyrimidin-2-yl)piperazine-1-carbonyl)- phenyl)-6-fluoro-1H-benzo[d]imidazole-4-carboxamide (11).....	37
5.1.11. 2-(4-(4-(5-(cyclopropylcarbamoyl)pyrimidin-2-yl)piperazine-1-carbonyl)phenyl)-6-fluoro-1H-benzo[d]imidazole-4-carboxamide (12).....	37
5.1.12. 6-fluoro-2-(4-(4-(5-(1-methyl-1H-pyrazol-4-yl)pyrimidin-2-yl)piperazine-1-carbonyl)phenyl)-1H-benzo[d]imidazole-4-carboxamide (13).....	38
5.1.13. 2-{4-[(1-[5-(cyclopropylcarbamoyl)pyrimidin-2-yl]azetid-3-yl)methyl]carbamoyl}phenyl}-1H-1,3-benzodiazole-4-carboxamide (14).....	38
5.1.14. 2-(4-{[(1-{5-[(oxetan-3-yl)carbamoyl]pyrimidin-2-yl}azetid-3-yl)methyl]carbamoyl}phenyl)-1H-1,3-benzodiazole-4-carboxamide (15).....	39
5.1.15. 2-{4-[(1-[4-(bicyclo[1.1.1]pentan-1-yl)carbamoyl]pyrimidin-2-yl]azetid-3-yl)methyl]carbamoyl}phenyl}-1H-1,3-benzodiazole-4-carboxamide (16).....	39
5.1.16. 4-(4-(4-Carbamoyl-1 <i>H</i> -benzo[ <i>d</i> ]imidazol-2-yl)benzoyl)piperazin-1-ium chloride (17).....	40
5.1.17. 4-(4-(4-carbamoyl-6-fluoro-1H-benzo[d]imidazol-2-yl)benzoyl)piperazin-1-ium dihydrochloride (18).....	41
5.1.18. 2-(4-{[(azetid-1-ium-3-yl)methyl]carbamoyl}phenyl)-4-carbamoyl-2,3-dihydro-1H-1,3-benzodiazol-1-ium dichloride (19).....	41
5.1.19. 4-carbamoyl-2-(4-{2,6-diazaspiro[3.3]heptan-6-ium-2-carbonyl}phenyl)-1H-1,3-benzodiazol-1-ium dichloride (20).....	42
5.1.20. 4-carbamoyl-2-(4-{[(piperidin-1-ium-4-yl)methyl]carbamoyl}phenyl)-1H-1,3-benzodiazol-1-ium dichloride (21).....	43
5.1.21. 4-carbamoyl-2-(4-{(3 <i>R</i> )-pyrrolidin-1-ium-3-yl]carbamoyl}phenyl)-1H-1,3-benzodiazol-1-ium dichloride (22).....	43



5.1.22. 4-carbamoyl-2-(4-{{(3S)-pyrrolidin-1-ium-3-yl}carbamoyl}phenyl)-1H-1,3-benzodiazol-1-ium dichloride ( <b>23</b> ).....	44
5.1.23. 4-(4-carbamoyl-1H-benzo[d]imidazol-2-yl)benzoic acid ( <b>24</b> ).....	45
5.1.24. 4-(4-carbamoyl-6-fluoro-1H-benzo[d]imidazol-2-yl)benzoic acid ( <b>25</b> )....	46
5.1.25. 2-(4-(4-(4-carbamoyl-1H-benzo[d]imidazol-2-yl)benzoyl)piperazin-1-yl)pyrimidine-5-carboxylic acid ( <b>26</b> ).....	46
5.1.26. N-(bicyclo[1.1.1]pentan-1-yl)-2-chloropyrimidine-4-carboxamide ( <b>27</b> )....	46
5.1.27. 2-chloro-N-cyclopropylpyrimidine-4-carboxamide ( <b>28</b> ).....	47
5.2. PARP Biochemical Assay.....	48
5.3. Determination of Aqueous Solubility and Stability.....	48
5.4. Kinase Panel Assay.....	48
5.5. Molecular Modeling.....	49

## LIST OF TABLES

Table 1. PARP1 inhibitory activity of benzimidazole-4-carboxamide analogues.....	8
Table 2. PARP1 inhibitory activity of 6-fluorobenzimidazole-4-carboxamide analogues.....	10
Table 3. PARP1 inhibitory activity of benzimidazole-4-carboxamide analogues with varying linkers.....	11
Table 4. PARP1 inhibitory activity of benzimidazole-4-carboxamide analogues with varying linker salts.....	12
Table 5. Solubility and Stability for Select Compounds.....	15
Table 6. PARP Isoform Screening of Selected Compounds ( <b>5, 8, 11, 12, 14, 16, 19, and 22</b> ).....	19
Table 7. Kinase Selectivity Profile of Selected Compounds ( <b>5, 6, 8, 9, 14, and 16</b> ).....	20

## LIST OF FIGURES

Figure 1. Block diagram of the PARP1 domains.....	1
Figure 2. Overlay of <b>1</b> bound to a constitutively.....	5
Figure 3. Lead Optimization Strategy.....	7
Figure 4. Binding model of <b>6</b> , <b>8</b> , <b>10</b> , and <b>16</b> .....	17
Figure 5. Binding model of <b>19</b> , <b>22</b> , and <b>23</b> .....	18
Figure 6. Mechanism of Synthesis for Boc-protected Intermediate.....	22
Figure 7. Mechanism for oxalyl chloride activated amide formation.....	24
Figure 8. NMR spectrum for N-{bicyclo[1.1.1]pentan-1-yl}-2-chloropyrimidine-4-Carboxamide ( <b>27</b> ).....	24
Figure 9. NMR spectrum for 2-(4-(4-(4-(bicyclo[1.1.1]pentan-1-ylcarbamoyl)pyrimidin-2-yl)piperazine-1-carbonyl)- phenyl)-1 <i>H</i> -benzo[ <i>d</i> ]imidazole-4-carboxamide ( <b>8</b> ).....	25
Figure 10. NMR spectrum for 2-{4-[(1-[4-({bicyclo[1.1.1]pentan-1-yl} carbamoyl)pyrimidin-2-yl]azetidin-3-yl}methyl)carbamoyl]phenyl}-1 <i>H</i> -1,3-benzodiazole-4-carboxamide ( <b>16</b> ).....	28

## LIST OF SCHEMES

Scheme 1. Synthesis of Compounds <b>2 – 9</b> .....	21
Scheme 2. Synthesis of Compounds <b>10 – 13</b> .....	26
Scheme 3. Synthesis of Compounds <b>14 – 16</b> .....	27
Scheme 4. Synthesis of Compounds <b>17 – 23</b> .....	28

## 1. INTRODUCTION

The family of poly(ADP-ribose) polymerase (PARP) proteins in humans constitute 17 members that contain a conserved catalytic domain (Figure 1).<sup>1,2</sup>

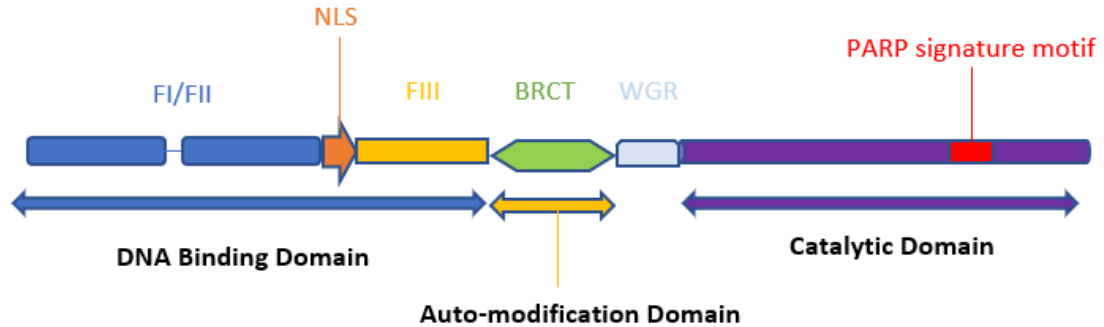


**Figure 1.** Block diagram of the PARP1 domains. From left to right: The DNA binding domain consists of three zinc finger motifs (FI-III) with evident PARP1 DNA-nick mediated activation. In between FII domain and FIII domain is the nuclear localization signal (NLS). The next domain is the automodification which consists entirely of the BRCT domain and plays a role in the auto-ADP-ribosylation as well as mediating some protein-protein interactions. Next to the BRCT domain is the WGR domain and finally the catalytic domain which handles ADP-ribose formation, elongation, and branching activity. Contained within the catalytic domain is the PARP signature motif present in both PARP1 and PARP2.<sup>3</sup>

Among these homologs, PARP1 and PARP2 have been extensively studied due to their involvement in the base excision repair (BER)-mediated DNA damage repair process.<sup>4,5</sup> The N-terminal DNA binding domain latches on to nicks formed throughout the DNA strand via the zinc finger motifs (FI-FIII). The C-terminal catalytic site of PARP1 participates in the hydrolytic cleavage of the  $\text{NAD}^+$  substrate into ADP-ribose and nicotinamide (NI). ADP-ribose units in the form of linear and branched chains are covalently transferred onto a wide range of target proteins such as histones, p53, topoisomerase I/II, DNA polymerases and DNA ligases (heteromodification) and onto PARP itself (automodification).<sup>6</sup> A post-translational modification, the poly-ADP-ribosylation (PARylation), of PARPs and other DNA repair proteins is imperative for

several biological functions, including DNA damage repair, genome integrity maintenance, cell differentiation, and cell proliferation.<sup>7,8</sup> PARylation of PARP1 is involved in non-covalent recruitment of DNA repair proteins such as XRCC1, DNA ligase III and DNA polymerase  $\beta$  (pol  $\beta$ ) to the sites of damaged DNA.<sup>9-11</sup>

Poly(ADP-ribosyl)ation is a crucial reaction that takes part in numerous physiological processes. These processes include inter- and intracellular signaling, transcription, DNA repair pathways, cell cycle regulation, mitosis, necrosis, and apoptosis.<sup>12</sup> PARP1 assists with the repair process for DNA that is damaged in general metabolic processes and other environmental factors. The overactivation of PARP1 causes a severe depletion in energy by consuming excess ATP. This will ultimately lead to necrotic cell death.<sup>13</sup> Since PARP1 activity is an expected result of malignant cancer cells, it is a prime target for study and inhibition.

A classic PARP inhibitor behaves as a NI mimic retaining the structural features of NI such as a carboxamide (primary or secondary) group bearing aromatic ring(s) with hydrophilic extensions orienting toward adenosine binding pocket (ABP) with appropriate linker groups.<sup>14</sup> Clinical development of PARP inhibitors (PARPi) is driven by two clinically validated therapeutic applications: (1) combination of PARPi with DNA damaging therapeutics (chemotherapy or radiotherapy) and (2) PARPi as a single-agent therapy to selectively eradicate the cancer cells carrying defective homologous recombination (HR) repair pathway (*BRCA1/2* mutant tumors).

A therapeutic strategy of combining PARPi with cytotoxic drugs such as DNA-methylating agents,<sup>15</sup> topoisomerase inhibitors,<sup>16</sup> platinum drugs,<sup>17</sup> and radiation<sup>18,19</sup> has demonstrated enhanced cytotoxic effects in numerous preclinical studies. Consequently,

this preclinical data allowed for the entry of PARPi into clinical trials as sensitizers of chemotherapy and radiotherapy in a wide array of tumor types.<sup>20</sup>

Undoubtedly, the use of PARPi as a single agent is touted as the most attractive approach based on the concept of synthetic lethality.<sup>21</sup> The term synthetic lethality refers to the exploitation of the tumor defect in HR double-strand breaks repair pathway with PARP inhibition as monotherapy.<sup>22,23</sup> It has been shown that HR defects are primarily restricted to tumors,<sup>24,25</sup> therefore, synthetic lethality by PARPi is likely to affect tumors over normal cells. Subsequently, a handful of PARPi were developed as cancer therapeutics either for combination with radiation therapy or cytotoxic drugs (e.g., temozolomide, cisplatin)<sup>26,27</sup> or as single agent therapies to kill cancer cells deficient in *BRCA1/2*-dependent DNA double-strand break repair mechanisms. Four PARPi (olaparib,<sup>28</sup> niraparib,<sup>29</sup> rucaparib,<sup>30</sup> and talazoparib<sup>31</sup>) entered the clinical stage as a single agent therapy for HR defective tumors. Veliparib<sup>17</sup> and many other PARPi (pamiparib,<sup>32</sup> stenoparib,<sup>33,34</sup> fluzoparib,<sup>35</sup> and mefuparib<sup>36</sup>) are undergoing multiple clinical trials. For chemical structures of these clinical PARPi refer to Velagapudi et al. published review.<sup>37</sup> These findings form a promising platform to develop new PARPi with high potency and unique allosteric-binding mechanism of PARP1 retention on DNA breaks as described in design rationale.

## 2. RESULTS AND DISCUSSION

### 2.1. Structure-Based Design of Highly Potent PARP1 Inhibitors Targeting ABP and $\alpha$ F-Helix

In the present study, we report the optimization of ABP motifs at the C2-position of our previously published benzimidazole-4-carboxamide (BI-4-CONH<sub>2</sub>) based lead compound **1** (PARP1, IC<sub>50</sub> = 2.6 nM) (Figure 1).<sup>38</sup> **1** proved to be a valuable lead compound as evidenced from: (i) a unique reverse allostery demonstrated by the compound leading to prolonged PARP1 retention on damaged DNA (pro-retention), unlike veliparib, which also consists of BI-4-CONH<sub>2</sub> as a NI mimic; (ii) a superior PARP-trapping ability over veliparib, yet inferior compared to a strong catalytic PARPi talazoparib;<sup>38</sup> (iii) its selectivity toward established anticancer targets PARP1, PARP2, TNKS1, and TNKS2 while sparing other catalytic PARP enzymes PARP3, PARP8, PARP10, and PARP14 unlike veliparib, when tested at 500 nM concentration. Although **1** had single-digit nM PARP1 inhibition, it showed moderate *BRCA*-dependent cytotoxic effect in SUM149 breast cancer cells, and this could be attributed to its poor cell permeability and water solubility. Another concern associated with **1** was the presence of a methyl ester which could be prone to hydrolysis thereby producing a carboxyl metabolite. This concern is supported by the fact that the carboxyl analogue showed a substantial loss of biochemical potency (Unpublished data). Therefore, further improvement in the metabolic stability, *BRCA*-driven cytotoxic effect, PARP-trapping potency, and drug-like properties is necessary to obtain candidate(s) suitable for further preclinical evaluation.



To understand the pro-retention of PARP1 on damaged DNA induced by **1** and to facilitate optimization of **1**, we obtained X-ray crystal structure of **1** bound to a constitutively active catalytic (CAT) domain of PARP1 (PDB ID: 6NTU), which was devoid of the helical domain (CAT $\Delta$ HD), and to a full length PARP1 (PDB ID: 6VKO) as overlaid in Figure 2.<sup>38</sup>

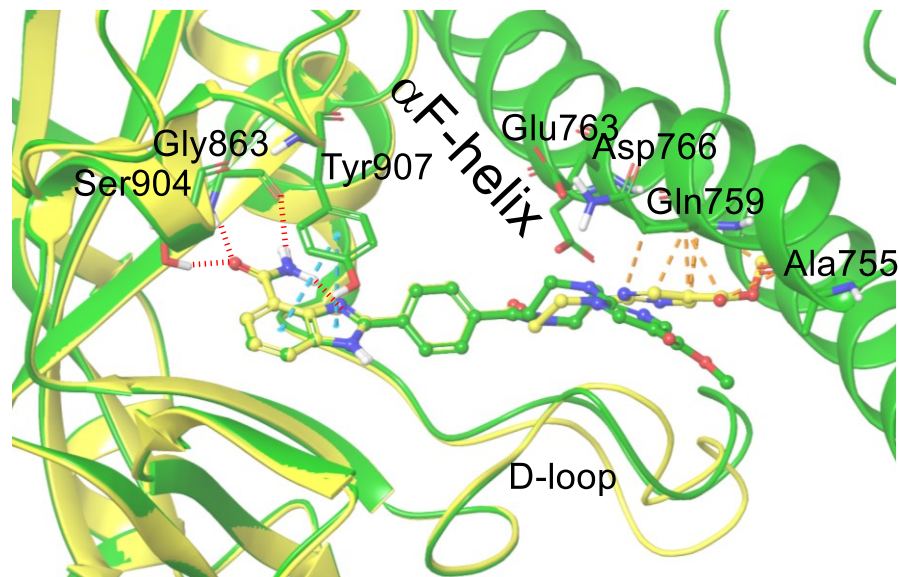


**Figure 2.** Overlay of **1** bound to a constitutively active catalytic (CAT $\Delta$ HD) domain of PARP1 (PDB ID 6NTU) devoid of the helical domain (HD) and to a full length PARP1 (PDB ID: 6VKO) shown respectively in yellow and green color illustrates the bent conformation of pyrimidine methyl ester moiety in the later induced by intact  $\alpha$ F-helix (steric clash indicated by broken orange lines). The binding model of **1** without the HD is shown in yellow and with the HD is shown in green.

Similar to veliparib, the BI-4-CONH<sub>2</sub> core of **1** forms three key hydrogen bonds with the backbone amide of Gly863 and the side chain of Ser904. Additionally, the benzimidazole ring is involved in the  $\pi$ - $\pi$  stacking with the side chain of Tyr907. The piperazine ring allows the pyrimidine ring of **1** to extend toward ABP, the region normally occupied by the HD in full length PARP1. To test the importance of the piperazine ring, a series of potent pyrimidine substituents were selected to be installed on an alternate linker i.e., aminomethylazetidine. In an effort to improve the flexibility, a

*sec*-amide was formed using aminomethylazetidine as the linker. A short series of compounds were tested for comparison with the piperazine linker found in **1**. In the full length PARP1-1 structure the methyl ester substituted pyrimidine moiety adopts a bent conformation compared to the one bound to CAT $\Delta$ HD PARP1. Our hypothesis that substituents on the pyrimidine ring will form a steric clash with  $\alpha$ F-helix and produce reverse allostery i.e., retention of PARP1 on DNA breaks was recently validated.<sup>38</sup> Hence, we seek to preserve this steric hindrance while conducting molecular modifications at 4- or 5-position of the pyrimidine ring to further improve the potency and drug-like properties of **1**. Despite a few early examples, these modifications mainly focus on different secondary amides featuring various ring substituents. This focus led to a significant increase in IC<sub>50</sub>, although the same issues of aqueous solubility and high molecular weight persist. In an attempt to remedy these issues, we explored the impact of truncating the molecule by removing the pyrimidine ring from **1**. This has allowed us to prepare a small library of compounds featuring various basic amine-functionalized saturated heterocycles as HCl salts. These set of compounds showed enhanced water solubility and stability over the extended analogues.

## **2.2. Structure-Activity Relationship**

The inhibitory activity of all target compounds was determined using PARP1 chemiluminescence assay.<sup>39</sup> Initially, compounds were screened at 5 nM concentration to analyze % inhibition of the PARP1 enzymatic activity. Compounds that met a specified biochemical % inhibitory potency threshold (>50%) were progressed to IC<sub>50</sub> determination in a ten-point biochemical concentration–response for PARP1 inhibitory

potency. The IC<sub>50</sub> values obtained for the positive controls veliparib and olaparib were comparable to previously reported values.<sup>39</sup>

### 2.2.1. Optimization of ABP-Binding Pyrimidine Tail Motif to Introduce Steric Clashes with $\alpha$ F-Helix of HD

In this study, we decided to explore the contribution of ABP-binding pyrimidine motifs on PARP1 inhibitory activity by varying the nature and position of R groups as well as removing the pyrimidine ring as shown in Figure 3.

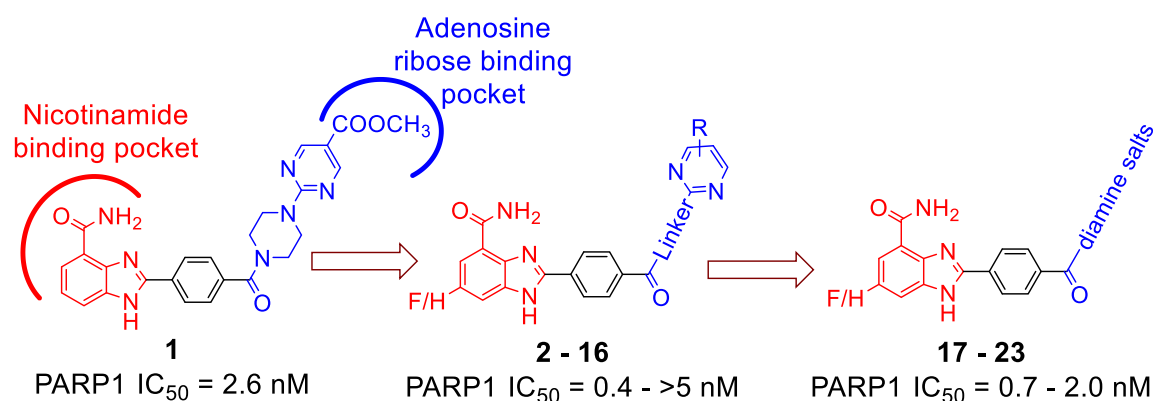
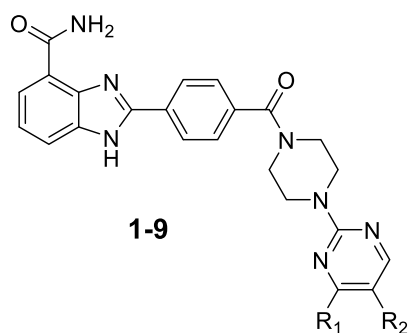


**Figure 3.** Lead optimization strategy to obtain potent and selective PARP1 inhibitors with unique PARP-trapping ability.

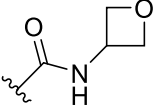
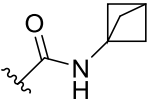
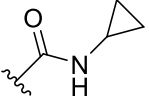
To execute this idea, we systematically optimized lead compound **1** (PARP1, IC<sub>50</sub> of 2.6 nM) (Table 1). **1** induced steric a clash with the  $\alpha$ F-helix portion of HD domain which resulted in pro-retention of PARP1 on damaged DNA and an increased cytotoxic activity as compared to veliparib. **1** was deprioritized because of its tendency to undergo hydrolysis under assay/physiological conditions. Moreover, the carboxyl analogue (IC<sub>50</sub> >10 nM), which is an expected metabolite of **1**, showed significant loss of PARP1 inhibitory potency (unpublished data). This observation indicated the existence of electrostatic repulsion in the ABP induced by acidic amino acid residues Glu763 and Asp766.

Replacement of an ester group in **1** with hydrolytically stable acetylene group (**2**, PARP1 54% inhibition at 5 nM) did not produce promising biochemical potency. This has prompted us to explore analogues that closely resemble **1** e.g., isosteric amide groups. Moreover, this choice was supported by the fact that acidic group was detrimental due to the repulsive effect exerted by ABP residues Glu763 and Asp766 on negatively charged groups of the ligands. The synthesis of the azetidine-*tert*-carboxamide analogue **3** led to a drastic decrease in the PARP1 biochemical potency compared to **1** (Table 1).

**Table 1. PARP1 inhibitory activity of benzimidazole-4-carboxamide analogues**



Comp. No.	R <sub>1</sub>	R <sub>2</sub>	PARP1 IC <sub>50</sub> (nM) <sup>a</sup>
<b>1</b>	H	-COOCH <sub>3</sub>	2.6
<b>2</b>	H	-C≡CH	~5 (54%) <sup>b</sup>
<b>3</b>	H		NA
<b>4</b>	H		>5
<b>5</b>	H		1.4
<b>6</b>	H		2.2

7	H		1.2
8		H	2.9
9		H	0.9
<b>Olaparib</b>	-	-	1.1
<b>Veliparib</b>	-	-	1.5

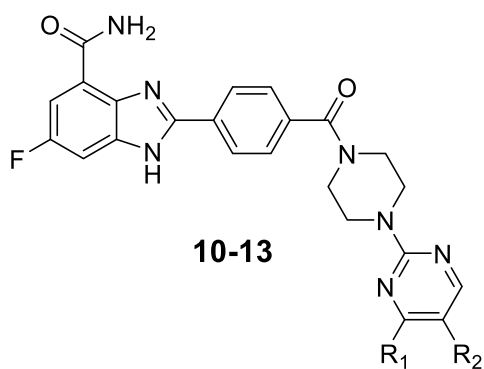
<sup>a</sup>Data shown are mean values obtained from two independent experiments performed in duplicates. <sup>b</sup>% inhibition screening at a single concentration (5 nM) was performed in duplicates and the IC<sub>50</sub> of all compounds with <50% inhibition was shown at >5 nM with % inhibition in parenthesis. NA – not active.

This result suggested that *sec*-amides might be favorable in the ABP of PARP1, and thus, subsequent analogues containing *sec*-amides were prepared. To that end, a *sec*-amide with an electronegative trifluoroethyl group gave **4** (45% inhibition at 5nM) showing less than desirable PARP1 inhibition. Next, we synthesized and tested a set of cyclopropyl amine-,<sup>40</sup> bicyclopentyl amine-<sup>41</sup>, and oxetanyl amine-derived secondary carboxamides **5**, **6**, and **7**. Each of these three compounds, **5** (IC<sub>50</sub> = 1.4 nM), **6** (IC<sub>50</sub> = 2.2 nM), and **7** (IC<sub>50</sub> = 1.2 nM), turned out to be very promising PARPi. Having established C5-pyrimidine carboxamides with favorable potency, we further investigated the effect of moving bicyclopentyl amine- and cyclopropyl amine-derived *sec*-carboxamide to the 4-position leading to **8** (IC<sub>50</sub> = 2.9 nM) as well as **9** (IC<sub>50</sub> = 0.9 nM) with the latter being more potent than its 5-position counterpart i.e., **5**.

**2.2.2. Investigation of the Fluorine Effect on Biochemical PARP1 Potency.** Previous work has reported that fluorine substituent *meta* to the carboxamide pharmacophore on NI mimic as in clinical PARPi (rucaparib,<sup>30</sup> talazoparib,<sup>31</sup> pamiparib,<sup>32</sup> and mefuparib<sup>36</sup>)

yielded into favorable biochemical and cellular potency against PARP1. Therefore, we strategically explored the installation of a fluorine atom at the 6-position of the BI-4-CONH<sub>2</sub> scaffold, leading to the identification of 6-fluoro derivatives **10** (IC<sub>50</sub> = 2.8 nM), **11** (IC<sub>50</sub> = 6.2 nM), **12** (IC<sub>50</sub> = 1.3 nM), and **13** (IC<sub>50</sub> = 1.3 nM) with a marginal loss of PARP1 inhibitory potency compared to non-fluorine counterparts except for **12** which showed comparable activity (Table 2).

**Table 2. PARP1 inhibitory activity of 6-fluorobenzimidazole-4-carboxamide analogues**



Comp. No.	R <sub>1</sub>	R <sub>2</sub>	PARP1 IC <sub>50</sub> (nM) <sup>a</sup>
<b>10</b>	H		2.8
<b>11</b>		H	6.2
<b>12</b>	H		1.3
<b>13</b>	H		1.3
<b>Olaparib</b>	-	-	1.1
<b>Veliparib</b>	-	-	1.5

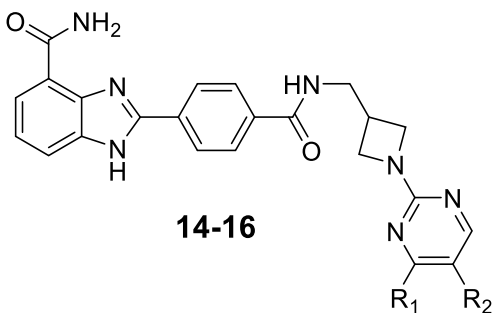
<sup>a</sup>Data shown are mean values obtained from two independent experiments performed in duplicates.

Although the fluorine substituent on the aromatic ring of the NI mimic has been shown to be favorable for PARP1 inhibition,<sup>42</sup> in this study it did not improve the potency compared to non-fluorine counterparts (**5**, **6**, **8**) with the exception of **13**. These findings suggest that the effect of a fluorine substituent on the NI mimic can be considered as contextual i.e., vary based on the type of NI mimic.

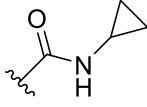
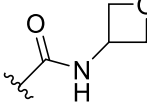
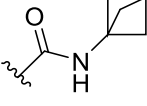
### 2.2.3. Effect of replacing the Piperazine linker with aminomethylazetididine

Further lead optimization strategy included investigation of drug-like piperazine ring surrogate i.e., 3-aminomethylazetididine in the active compounds identified in the piperazine series. The primary strategy with replacing the piperazine ring with aminomethylazetididine was to change the *tert*-amide of the linker to a *sec*-amide. This allows for much more flexibility as opposed to the relatively flat scaffold of the piperazine linker (Table 1). The lead substituents identified in the first series of compounds (cyclopropylamide, oxetanamide, and *meta*-bicyclopentamide) were similarly installed on the new linker. This led to the identification of compounds **14** (IC<sub>50</sub> = 0.5 nM), **15** (IC<sub>50</sub> = 0.4 nM), and **16** (IC<sub>50</sub> = 0.7 nM) (Table 3).

**Table 3. PARP1 inhibitory activity of benzimidazole-4-carboxamide analogues with varying linkers**



Comp. No.	R <sub>1</sub>	R <sub>2</sub>	PARP1 (nM) <sup>a</sup>	IC <sub>50</sub>
<b>14</b>				0.5
<b>15</b>				0.4
<b>16</b>				0.7

14	H		0.5
15	H		0.4
16		H	0.7
<b>Olaparib</b>	-	-	1.1
<b>Veliparib</b>	-	-	1.5

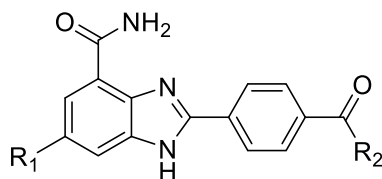
<sup>a</sup>Data shown are mean values obtained from two independent experiments performed in duplicates.

The new linker shows substantially increased activity to the piperazine-linker counterparts **5**, **7**, and **8**, with each analogue showcasing sub-nanomolar IC<sub>50</sub> values. These results potentially show the importance of the improved flexibility in the middle of the ligand structure.

#### 2.2.4. Drug-like derivatives of BI-4-CONH<sub>2</sub> scaffold

Despite extraordinary biochemical PARP1 inhibitory potency exhibited by above-mentioned PARP1 inhibitors, they suffer from number of issues e.g., high MW and poor aqueous solubility. To address these issues, we truncated the molecule by removing pyrimidine (Table 4).

**Table 4. PARP1 inhibitory activity of benzimidazole-4-carboxamide analogues with varying linker salts**



**17-23**

Comp. No.	R <sub>1</sub>	R <sub>2</sub>	PARP1 IC <sub>50</sub> (nM) <sup>a</sup>
-----------	----------------	----------------	--



<b>17</b>	H		1.5
<b>18</b>	F		2.0
<b>19</b>	H		0.7
<b>20</b>	H		1.3
<b>21</b>	H		1.0
<b>22</b>	H		1.0
<b>23</b>	H		1.3
<b>Olaparib</b>	-	-	1.1
<b>Veliparib</b>	-	-	1.5

<sup>a</sup>Data shown are mean values obtained from two independent experiments performed in duplicates.

Not only will this limit the molecular weight of the molecule by eliminating the necessity for decorated pyrimidine rings, but it will drastically improve aqueous solubility by utilizing hydrochloride salt. The first derivative piperazine salt (**17**, IC<sub>50</sub> = 1.5 nM) gave PARP1 inhibition similar to that observed for most active compounds carrying pyrimidine extensions. Next, the 6-fluoro substituted piperazine salt (**18**, IC<sub>50</sub> = 2.0) was evaluated to further study the effect of fluorine on PARP1 inhibition. Encouraged by the relative activity of the truncated compound, we explored several piperazine ring surrogates. Since the aminomethylazetidine linker was already shown to significantly improve potency over compounds with the piperazine linker, it was tested as a hydrochloride salt (**19**, IC<sub>50</sub> = 0.7 nM). In this case, the activity was significantly

improved over both piperazine salts (**17** and **18**), and more like those analogues containing aminomethylazetidione as a linker (Table 3). With the truncated compounds now showing the potential to exhibit similar potency as the pyrimidine-containing compounds, a series of *sec*-amides and an additional *tert*-amide was synthesized to fully explore the potential of a truncated structure (Table 4). This series led to the identification of four compounds. The first being Compound **20**, representing the lone *tert*-amide for this series, which did not show any improvement in activity compared to the piperazine analogues. **20** also showed a substantial decrease in activity when compared to the **19**. With this in mind, the decision was made to focus on *sec*-amides for the remainder of the series, which led to identification of **21** ( $IC_{50} = 1.0$  nM), **22** ( $IC_{50} = 1.0$  nM), and **23** ( $IC_{50} = 1.8$  nM). Each of the new analogues showed comparable activity with the most active compound of this series (**19**), apart from **23** which showed a notable decrease in activity to its *R*-isomer counterpart, **22**.

### **2.3. In Vitro ADME Parameters of Selected Compounds (5, 6, 7, 9, 12, 14, 15, 17, 18, 19, 21, and 22)**

To test the extent to which the solubility and stability was improved throughout the structural modifications, a solubility experiment was performed with representative compounds from each series (Table 5). As expected, the first series showed both poor solubility and stability. For example, the 5-position cyclopropyl carboxamide (**5**) demonstrated poor solubility of 12.9  $\mu$ M and 4.9  $\mu$ M at pH 4.0 and 7.4, respectively. Maintaining the cyclopropyl carboxamide but adding fluorine to the 5-position of benzimidazole (**12**) showed a slight increase in solubility at pH 4.0 whereas the solubility

at 7.4 did not substantially change. However, the stability of **12** at pH 7.4 did improve quite a bit increasing to 61% parent compound in solution as opposed to just 44% for **5**.

**Table 5. Solubility and Stability for Select Compounds**

Compd	Aqueous solubility <sup>a</sup> ( $\mu$ M) pH4/7.4	Chemical stability at pH7.4 (%) (24h)
<b>1</b>	11.3/7.6	31
<b>5</b>	12.9/4.9	44
<b>6</b>	14.8/12.3	50
<b>7</b>	13.2/7.5	52
<b>9</b>	13.5/10.1	49
<b>12</b>	12.8/9.6	61
<b>14</b>	26.9/17.3	67
<b>15</b>	21.8/20.1	69
<b>17</b>	1508/1442	98
<b>18</b>	1925/1758	92
<b>19</b>	2235/1833	95
<b>21</b>	1870/1377	96
<b>22</b>	1882/1670	99
Veliparib	-	-

<sup>a</sup>Aqueous solubility is determined by a 24 h shake flask thermodynamic solubility method in PBS buffer at pH 4 and 7.4. Stability was determined via the same method as solubility in PBS buffer at pH 7.4.

The first notable change in solubility came when switching the piperazine linker to aminomethylazetidine linker. In this case, the cyclopropyl carboxamide analogue for this series (**14**) showed an almost two-fold increase in solubility versus the piperazine analogues. This is while also showing a slight increase in stability with 67% parent compound in solution. Finally, the truncated series (Table 4) was evaluated for solubility and stability. As expected, this series showed drastic improvement in both solubility and stability. For example, the piperazine analogue without fluorine (**17**) is almost 117-fold

more soluble than the decorated pyrimidine counterpart. This pattern is consistent with each of the salt analogues.

With this data in mind, it does not seem that changing the carboxamide on the decorated pyrimidine has a significant effect on the solubility or stability of the compounds. A much more significant improvement is achieved by changing the linker to improve flexibility and three-dimensionality within the center of the compound as evidenced by the improvement between the first two series and the third. Although, this improvement is made trivial by the sharp increase seen in the salt-analogues.

#### **2.4. Binding Model for Key Compounds within the active site of PARP1**

In order to examine the particular interactions and how they change with each modification, a series was chosen to evaluate through simulated interactions via molecular modeling. The first series that was explored was pyrimidine decorated with bicyclopentyl carboxamide in both the 4- and 5-position of pyrimidine (Figure 4). Each ligand exhibited the same pattern of interactions on the left-hand portion of the compound. The primary carboxamide forms three hydrogen bonds with Gly863 and Ser904. The other conserved interaction is the  $\pi$ - $\pi$  stacking exhibited between Tyr907 and benzimidazole ring. The only major difference between the four binding models is the extra interaction showcased by the 4-position amide proton with Ala755. This hydrogen bond is not present in the 5-position carboxamide and is present in all 4-position carboxamides regardless of linker or a change in ring structure from bicyclopentyl to cyclopropyl (not pictured). This extra hydrogen bond can potentially explain the increased inhibitory activity for each 4-position analogue in the first series (Table 1). The addition of fluorine does not seem to create any new interactions but the strong electron-

withdrawing characteristic of fluorine on the benzimidazole ring will increase the strength of the  $\pi$ - $\pi$  stacking between the benzimidazole ring and Tyr907. Lastly, the aminomethylazetidine linker shows improved flexibility in the bent conformation as anticipated. The orientation of the azetidine ring allows for extra van der Waals interactions that are not present with the piperazine linker.

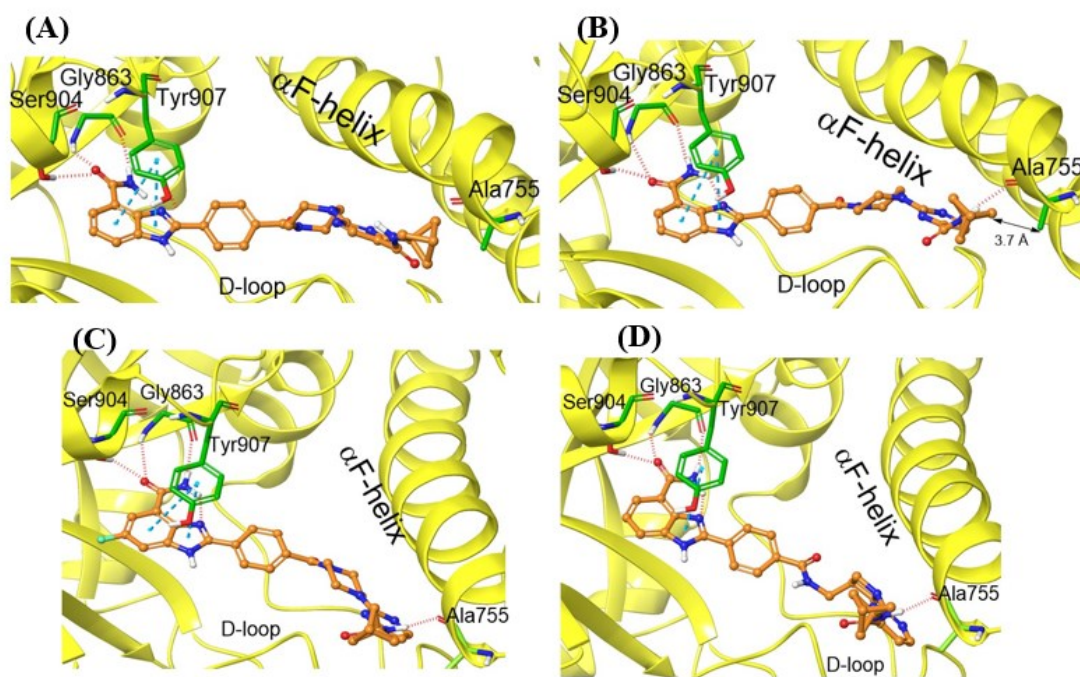


**Figure 4.** Binding model of **6** (A), **8** (B), **10** (C), and **16** (D) within the active site of PARP1. Inhibitor is shown in ball and stick model. Broken red lines indicate hydrogen bonds and broken cyan line shows  $\pi$ - $\pi$  stacking.

The next series of compounds involved truncating the structure by removing the pyrimidine, thus resulting in an entirely different conformation within the binding pocket of PARP1 (Figure 5). These compounds bend in a different position as the pyrimidine series. This causes the ligand to interact with a completely different section of the  $\alpha$ F-helix. The most common new interaction conserved between the various salt analogues, including those not pictured, is the strong ionic interaction between Glu763 and the secondary amine. In fact, this ionic interaction may be the reason why inhibition is in

general just as good as the lead compounds from the pyrimidine series. This is supported by the substantial loss in activity between the **22** and **23** isomers of the pyrrolidine salt. The (*S*)-isomer (**23**) bends away from Glu763 and forms a weak ionic interaction with Asp766. The distance between Asp766 and the amine is 4.8Å whereas the distance from Glu763 to the (*R*)-isomer (**22**) is 2.8Å.

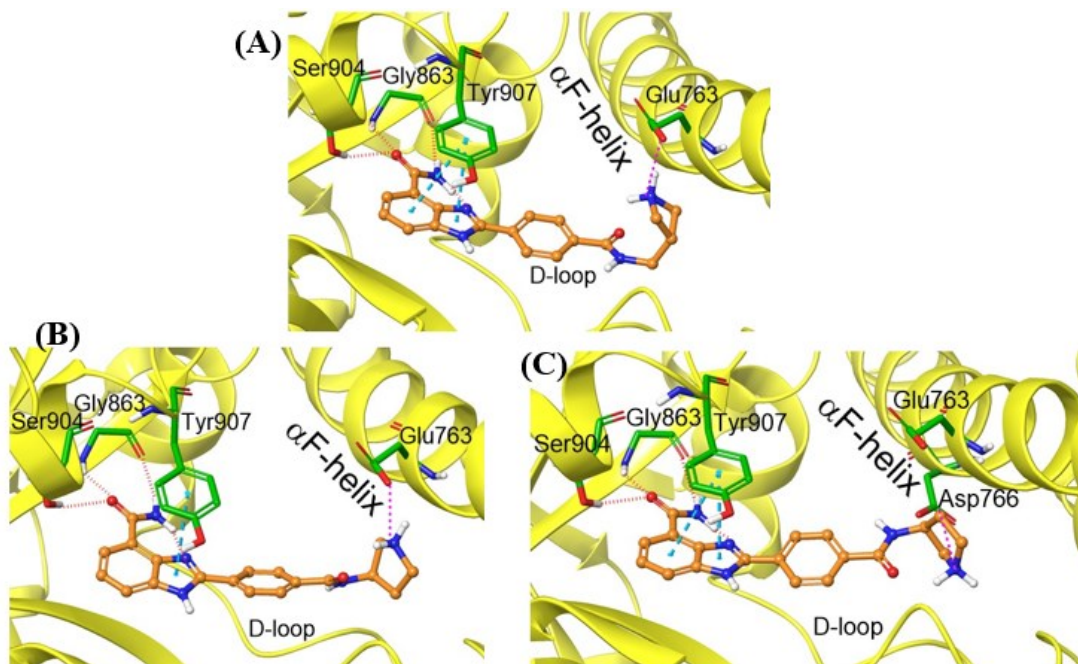


**Figure 5.** Binding model of **19** (A), **22** (B), and **23** (C) within the active site of PARP1. Inhibitor is shown in ball and stick model. Broken red lines indicate hydrogen bonds, broken cyan line shows  $\pi$ - $\pi$  stacking, and broken pink line reveals ionic interaction.

### 2.5. Specificities and Off-Targets within the PARP family.

Since the majority of clinically validated PARPi possess a wide spectrum of inhibitory activity toward multiple PARPs, we wanted to evaluate the selectivity profile of the best set of representative PARPi against a panel of PARPs (Table 6). Based on the inhibition profile obtained at 100 nM concentration, **5-22** showed near complete inhibition of the activity of clinically relevant PARP family members such as PARP2, TNKS1, and TNKS2 with relatively little to no effect on PARP3, PARP6, PARP7,

PARP8, PARP10 and PARP14. This data is of clinical significance because TNKS1/2, similar to PARP1 and PARP2, are involved in cancer pathogenesis.<sup>33</sup>

**Table 6. PARP Isoform Screening of Selected Compounds (5, 8, 11, 12, 14, 16, 19, and 22)**

Compound	% PARP inhibition at 100 nM								
	PARP2	PARP3	TNKS1	TNKS2	PARP6	PARP7	PARP8	PARP10	PARP14
5	99	NA	91	96	NA	NA	NA	NA	NA
8	100	NA	74	96	NA	NA	NA	NA	NA
11	98	NA	86	98	NA	40	NA	NA	NA
12	98	NA	100	96	NA	36	NA	NA	NA
14	98	NA	96	94	NA	NA	NA	NA	NA
16	98	NA	95	97	NA	NA	NA	46	NA
19	99	NA	74	88	NA	45	NA	NA	NA
22	100	NA	64	84	NA	NA	NA	NA	NA
Veliparib	100	57	NA	38	NA	NA	NA	NA	NA

<sup>a</sup> Veliparib were used as a reference compound

## 2.6. Kinase Panel Assay

Considering the occurrence of off-target kinase inhibition by some of the FDA approved PARPi,<sup>43</sup> we decided to explore whether our selected set of PARPi have any off-target kinase inhibition. To that end, we screened compounds **5, 6, 8, 9, 14, and 16** against a panel of 12 kinases belonging to either Ser/Thr or tyrosine kinases (Table 6). We used 100 nM of selected compounds at the Km concentration of ATP, and the kinase activity was expressed as a percentage inhibition of each enzyme in the presence of selected compound. Interestingly, none of the PARPi have any noticeable inhibitory effect against tested kinases.

**Table 7. Kinase Selectivity Profile of Selected Compounds (5, 6, 8, 9, 14, and 16)**

Kinase	<b>5</b> %inhibiti on at 100 nM	<b>6</b> %inhibiti on at 100 nM	<b>8</b> %inhibiti on at 100 nM	<b>9</b> %inhibiti on at 100 nM	<b>14</b> %inhibiti on at 100 nM	<b>16</b> %inhibiti on at 100 nM
CHK1	-5	0	0	-1	2	5
DNA- PK	2	2	1	3	2	2
FLT3	9	9	9	7	8	8
JAK2	7	5	5	5	6	2
KIT	17	8	15	10	11	13
cMet	1	2	2	5	1	0
CDK6	-3	-5	0	-5	-2	-3
PIK3C2 A	7	3	6	-2	-2	-1
TLK1	-14	13	2	-8	-9	-5
ULK1	2	2	1	1	1	0
ULK2	1	1	3	3	3	-1
Wee1	-12	-8	-13	-9	-12	4

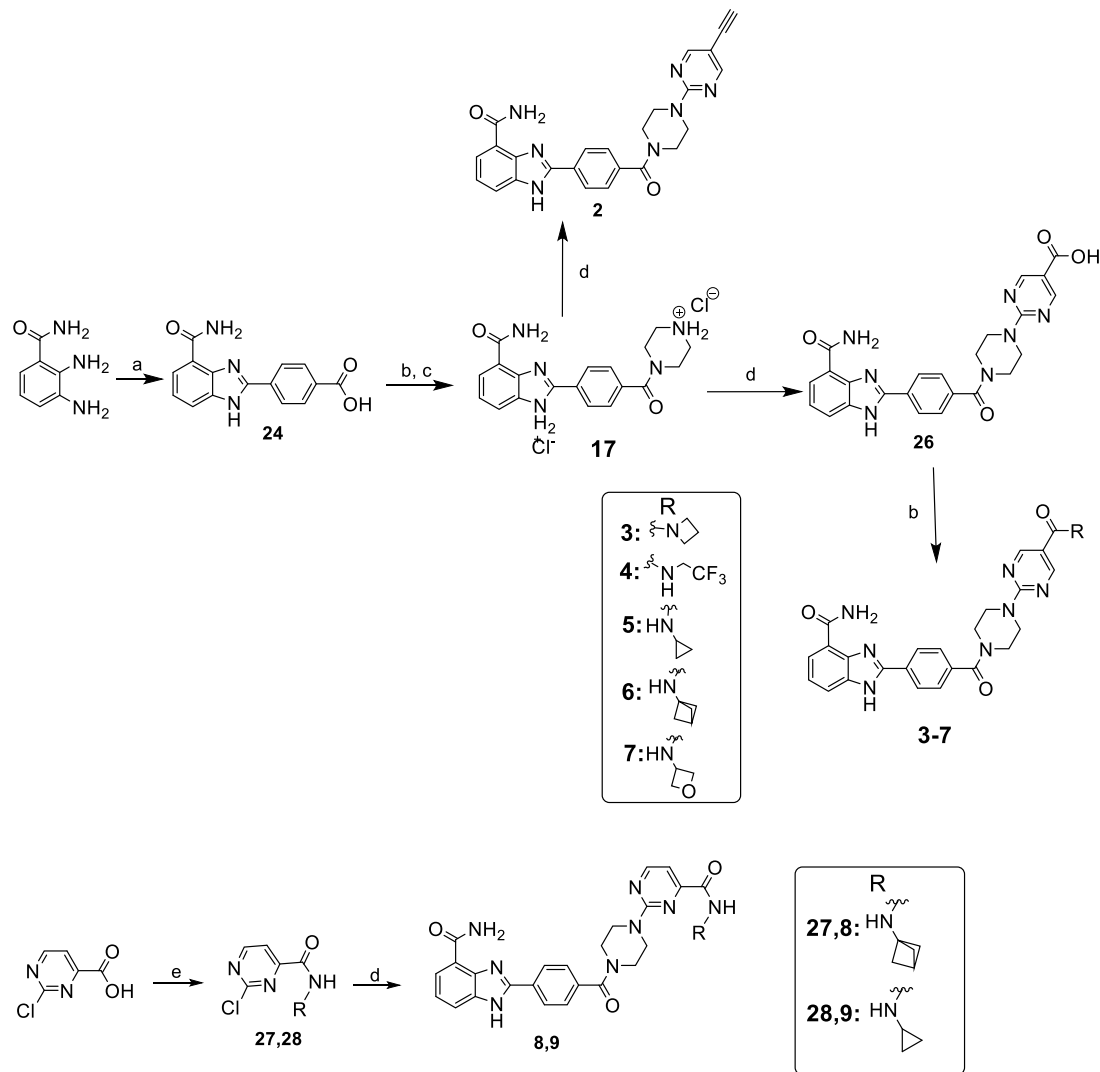
<sup>a</sup> % inhibition of kinase activity at ATP concentrations close to the  $K_m$  of each tested kinase from triplicate was obtained using Thermo Fisher Scientific's Select screen service.



### 3. CHEMISTRY

Synthesis of target compounds **2–9** and **17** mentioned in Table 1 is depicted in Scheme 1. Initially, key intermediate acid **24** was prepared from 2,3-diaminobenzamide and 4-formylbenzoic acid via ammonium acetate assisted condensation reaction (Scheme 1).<sup>44</sup>

#### Scheme 1. Synthesis of Compounds **2–9**



“Reagents and conditions: (a) 4-formylbenzoic acid, NH<sub>4</sub>OAc, DMF, 100 °C, 6 h, 86%; (b) appropriate primary/secondary amines, HBTU, DIPEA, DMF, 0 °C to rt, overnight, 28–85%; (c) conc. HCl, dioxane/DCM, rt, 6h 87%; (d) **17**, appropriate substituted 2-chloropyrimidines or synthesized pyrimidine, DIPEA, dioxane/DMF (9:1), microwave, 160 °C, 45–60 min, 39–67%; (e) (i) oxalylchloride, catalytic DMF, DCM, reflux, 2 h; (ii) appropriate primary amines, Et<sub>3</sub>N, THF, 0 °C to rt, overnight, 28–31%.

With the development of interest to further expand our library for structural diversity around the pyrimidine motif, we initially coupled the acid, **24**, with *N*-Boc piperazine to give the Boc-protected amide intermediate (for reaction mechanism see Figure 6), which was then treated with HCl to obtain the amine hydrochloride salt, **17**. *N*-Arylation could be achieved by heating **17** with the requisite 2-chloropyrimidine under microwave irradiation and DIPEA in 1,4-dioxane (modified S<sub>N</sub>Ar reaction conditions) to obtain compound **2**.<sup>45</sup>

### Reaction Mechanism for HBTU-mediated Peptide Coupling

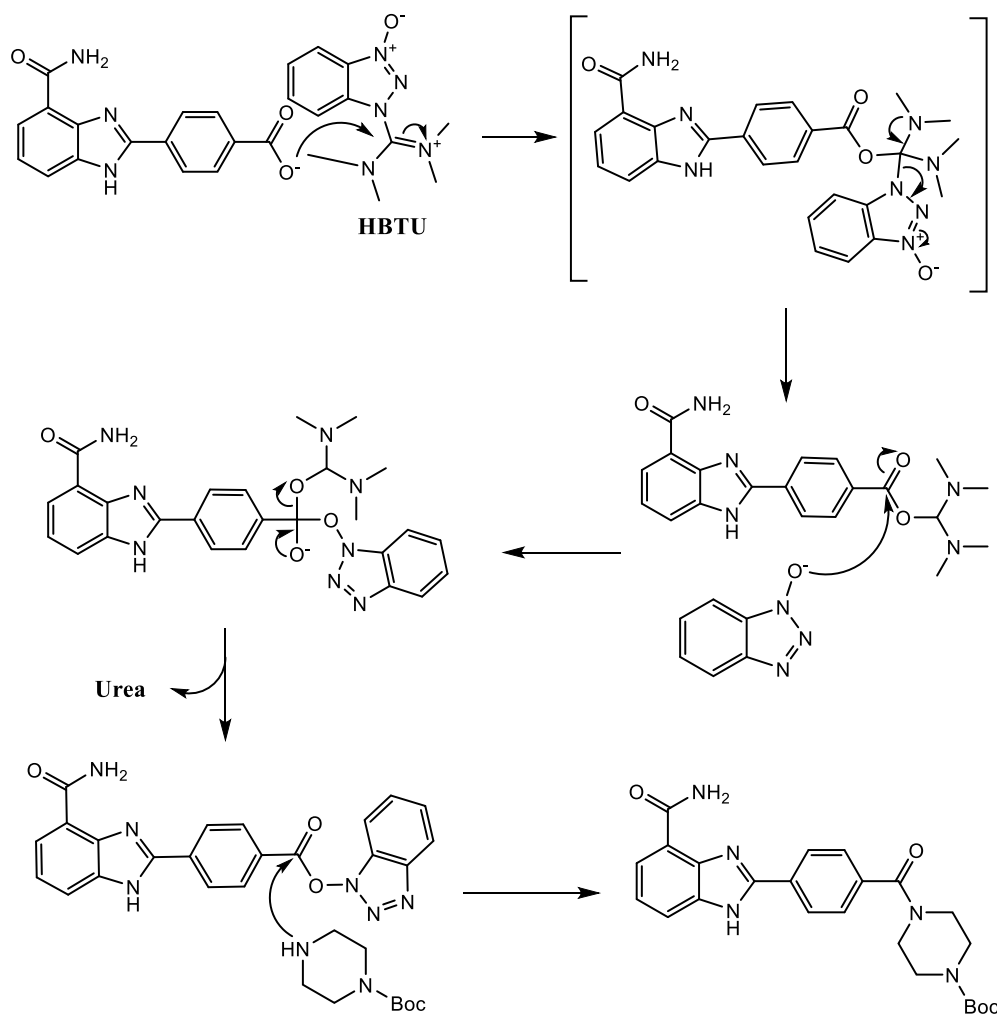


**Figure 6.** Mechanism of synthesis for boc-protected intermediate.<sup>46</sup>

Synthesis of the remaining target compounds of Table 1 featuring wide range of substituted carboxamides on the pyrimidine ring is outlined in Scheme 1. The required acid intermediate (**26**) was prepared by reacting 2-chloropyrimidine-5-carboxylic acid with amine salt **17**. Subsequently, acid **26** was coupled with a set of primary/secondary amines using HBTU and DIPEA to obtain pyrimidine-5-carboxamide functionalized compounds **3–7**.<sup>44</sup>

Insertion of the bicyclo[1.1.1]pentylamine and cyclopropylamine-derived carboxamide at C4-pyrimidine turned out to be a challenging substrate under conventional HBTU coupling conditions. The closer proximity to the nitrogen in the pyrimidine ring is believed to have reduced the reactivity of the carboxyl group. Due to the high reactivity of acid chlorides, we followed an alternate protocol wherein 2-chloropyrimidine-4-carboxylic acid was first converted to the corresponding amides via activated acid chloride and subsequently coupled with the appropriate amines to afford intermediates **27** and **28** (for reaction mechanism see Figure 7). Following the modified S<sub>N</sub>Ar reaction with amine salt **17** furnished target compounds **8** and **9**. See Figure 8 for representative NMR spectra of intermediate **27** and Figure 9 for final compound **8**.

## Mechanism for Oxalyl Chloride Activated Amide Formation

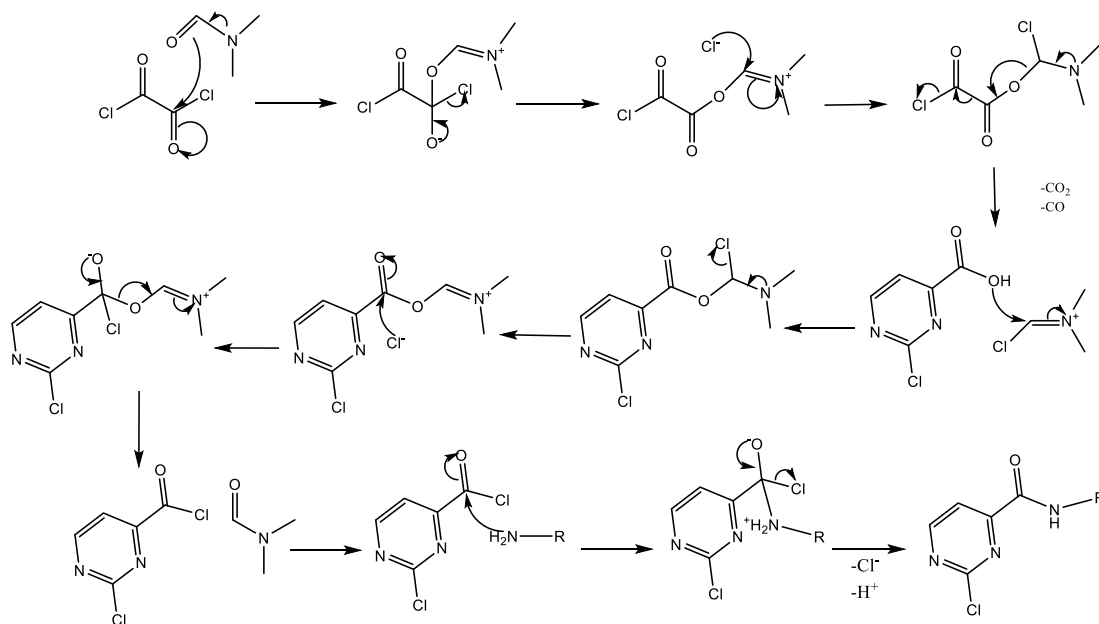


**Figure 7.** Mechanism for oxalyl chloride activated amide formation<sup>47</sup>

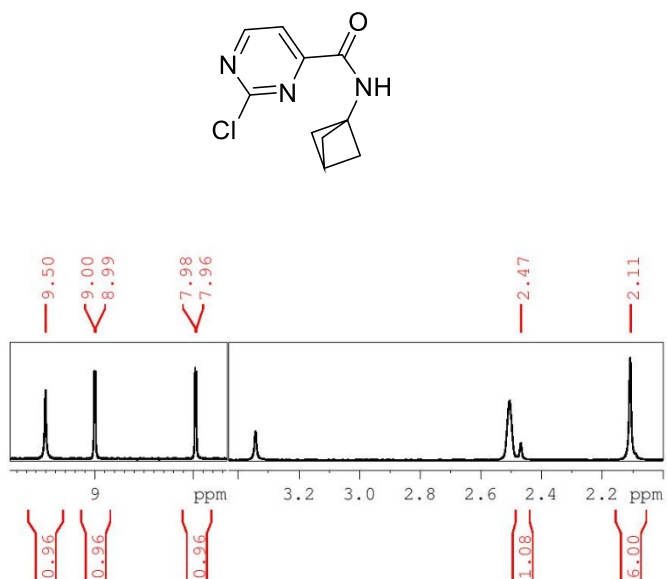


**Figure 8.** NMR spectrum for *N*-(bicyclo[1.1.1]pentan-1-yl)-2-chloropyrimidine-4-carboxamide (27). All relevant signals are integrated, and positions are marked according to the ppm at which they appear. The single amide proton appears as a singlet at 9.50 ppm, and both protons on the pyrimidine ring are represented as two doublets appearing at 9.0 ppm and 7.98 ppm respectively. The six protons on the secondary carbons in bicyclo[1.1.1]pentane appear as one singlet at 2.11 ppm and the remaining tertiary carbon appears as a singlet partially obscured by the DMSO solvent signal at 2.47 ppm.

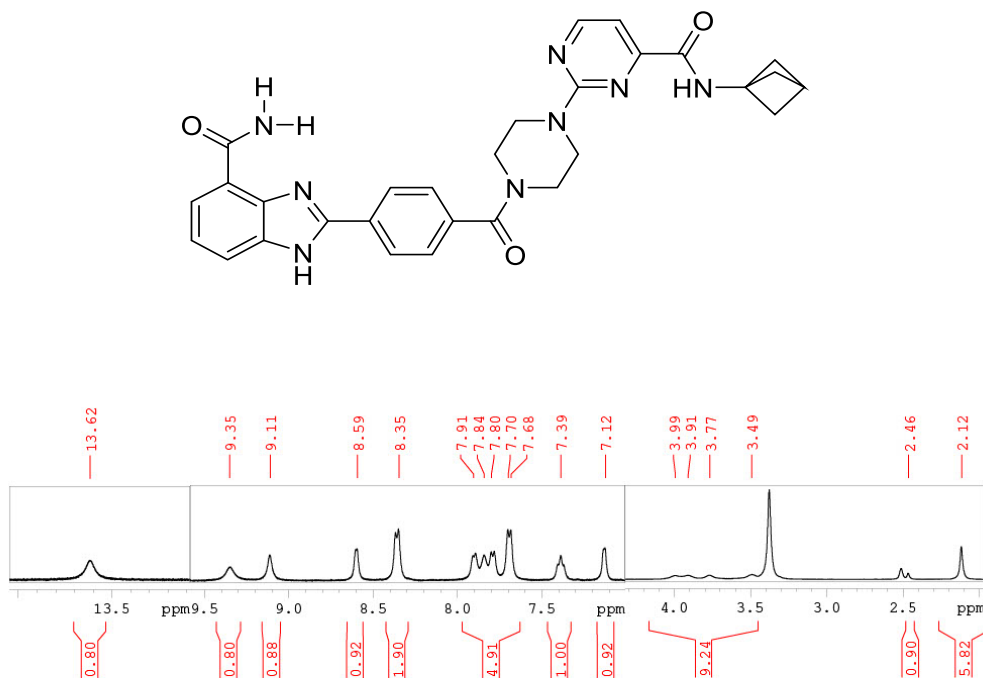
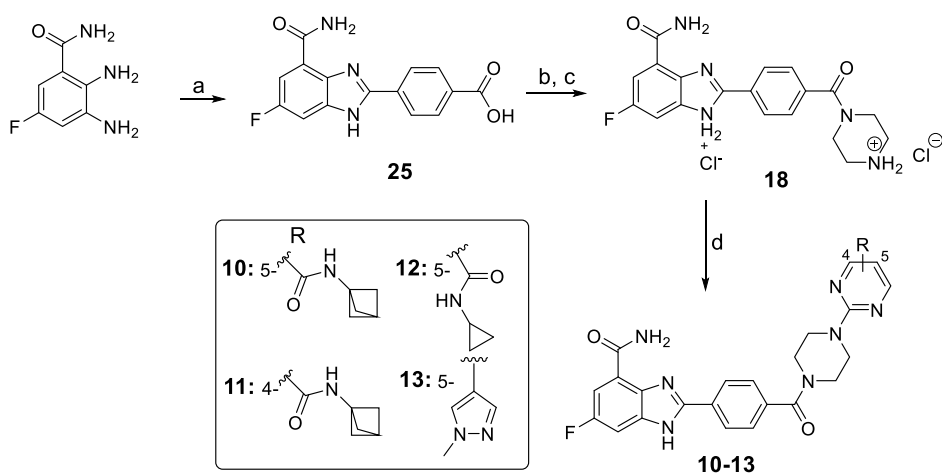


**Figure 9.** NMR spectrum for 2-(4-(4-(4-(bicyclo[1.1.1]pentan-1-ylcarbamoyl)pyrimidin-2-yl)piperazine-1-carbonyl)-phenyl)-1H-benzo[d]imidazole-4-carboxamide (**8**). All relevant signals are integrated, and positions are marked according to the ppm at which they appear. The furthest signal downfield at 13.62 ppm represents the secondary amine at the 3-position of benzimidazole. Both singlets at 9.35 and 9.11 correspond to amide protons, one from the primary amide on the benzimidazole scaffold and one from the *N*-{bicyclo[1.1.1]pentan-1-yl}-2-chloropyrimidine-4-Carboxamide identified in Figure 5. The same doublets identified in Figure 5 on the pyrimidine ring are present at 8.59 ppm and 7.12 ppm respectively. The four protons on the benzene ring split into two doublets at 8.35 ppm and 7.70 ppm. The second amide proton from the benzimidazole carboxamide resonates as a singlet at 7.84 ppm along with the 6- and 4-position protons on the benzimidazole benzene at 7.91 ppm and 7.80 ppm respectively as doublets. The final proton in the aromatic region is the 5-position proton of benzimidazole which appears as a triplet at 7.39 ppm. The four broad peaks of piperazine, corresponding to each secondary carbon, appear at 3.99, 3.91, 3.77, and 3.49. The bicyclopentane protons appear in almost the exact position as in figure 5.

Next, we decided to introduce a fluorine atom at 6-position of the BI-4-CONH<sub>2</sub> scaffold containing compounds listed in Table 2. To that end, the 2,3-diamino-5-

fluorobenzamide was condensed with 4-formylbenzoic acid to afford acid **25**. Next, amide coupling proceeded smoothly with the *N*-Boc piperazine to obtain corresponding *N*-Boc amide intermediate, which underwent Boc deprotection to furnish amine salt **18**. Finally, the amine was *N*-arylated in the usual manner with structurally diverse 2-chloropyrimidines to obtain **10–13** (Scheme 2).

### Scheme 2. Synthesis of Compounds 10–13

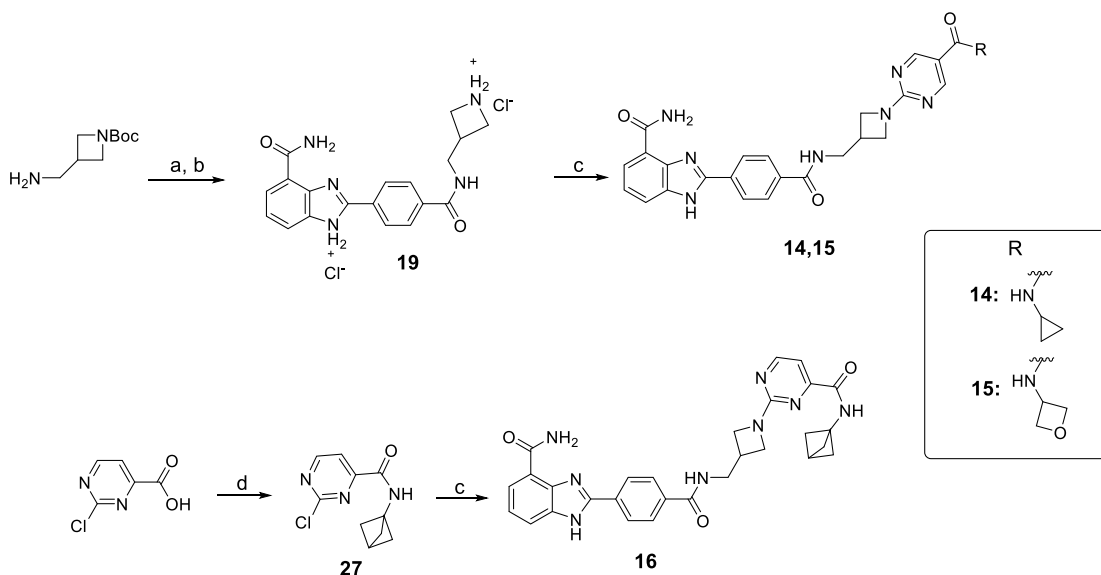


<sup>a</sup>Reagents and conditions: (a) 4-formylbenzoic acid, NH<sub>4</sub>OAc, DMF, 100 °C, 7 h, 80%; (b) *N*-Boc piperazine, HBTU, DIPEA, DMF, 0 °C to rt, overnight, 79%; (c) 4 N HCl/dioxane, DCM, 0 °C to rt, 6 h, 81%; (d) appropriate substituted 2-chloropyrimidines, DIPEA, dioxane/DMF (9:1), microwave, 160 °C, 45–60 min, 33–37%.

Additionally, we investigated the effect of replacing the piperazine linker with aminomethylazetidine, which led to synthesis of target compounds **14–16** of Table 3. A representative NMR spectra for this series can be seen in Figure 10. The salt intermediate (**19**) was prepared in a similar way as the piperazine salt (**17**). Subsequently, the amine salt was coupled with corresponding 4- and 5-chloropyrimidine carboxamides. Both the cyclopropane (**14**) and oxetane (**15**) C5-pyrimidine carboxamides were prepared via the

standard HBTU method mentioned in Scheme 1. The C4-bicyclopentamine-substituted pyrimidine, **16**, was prepared via the same method as described for **8** (Scheme 3).

### Scheme 3. Synthesis of Compounds 14–16



“Reagents and conditions: (a) **24**, HBTU, DIPEA, DMF, 0 °C to rt, overnight, 86%; (b) conc. HCl, dioxane/DCM, rt, 6h, 73%; (c) **19**, appropriate substituted 2-chloropyrimidine carboxamides, DIPEA, dioxane/DMF (9:1), microwave, 160 °C, 45–60 min, 35–40%; (d) (i) oxalylchloride, catalytic DMF, DCM, reflux, 2 h; (ii) bicyclo[1.1.1]pentylamine, Et<sub>3</sub>N, THF, 0 °C to rt, overnight, 32%.

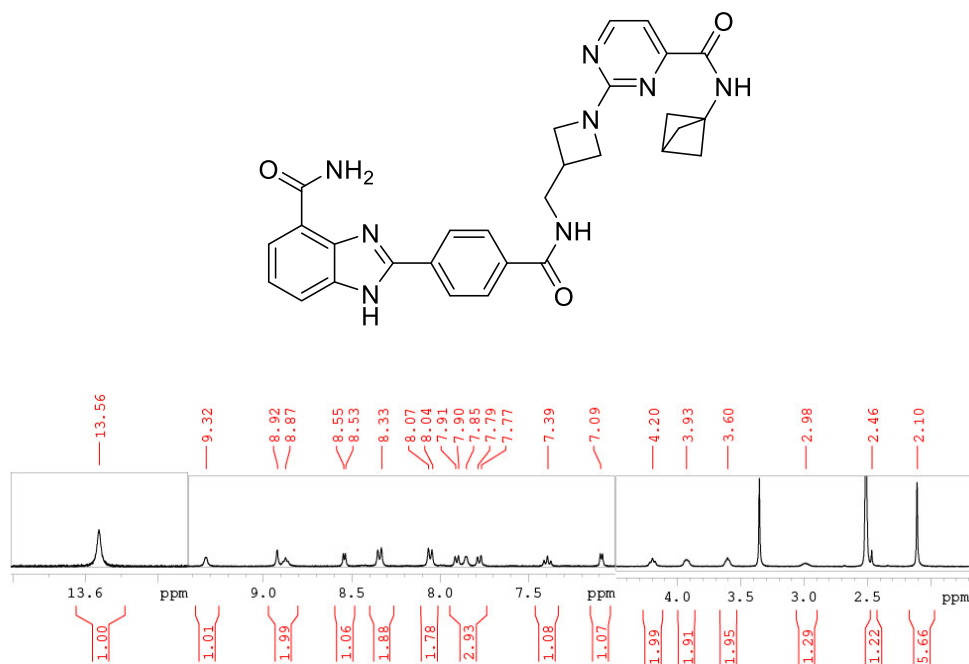
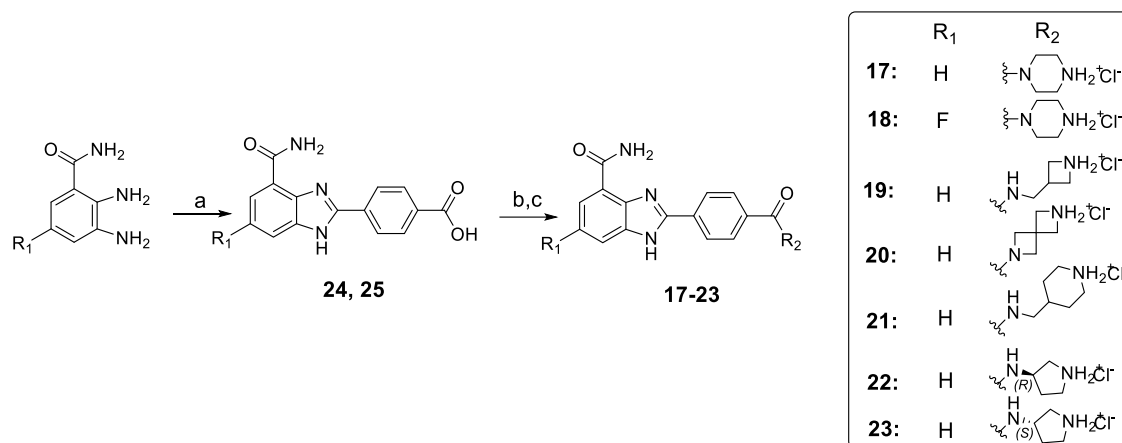


**Figure 10.** NMR spectrum for 2-{4-[(1-[4-({bicyclo[1.1.1]pentan-1-yl}carbamoyl)-pyrimidin-2-yl]azetidin-3yl)methyl]carbamoyl]-phenyl}-1H-1,3-benzodiazole-4-carboxamide (**16**). Most signals are conserved from figure 6 with some variation in the ppm a particular signal appears, for example the signal at 7.70 ppm in figure 6 now resonates at 8.07. The biggest difference between the two spectra between the 7.00 ppm and 10.00 ppm range is an extra amide proton at 8.87 ppm from the aminomethylazetidine linker. The rest of the linker protons show up at 4.20, 3.93, 3.60, and 2.98 ppm.

Lastly, various piperazine replacements were tested as salts alongside the original piperazine salt (**17**) as well as the 6-position fluoro-piperazine salt (**18**). Each was prepared by the same method as **17** to afford target compounds **19-23** (Scheme 4).

#### Scheme 4. Synthesis of Compounds 17-23



<sup>a</sup>Reagents and conditions: (a) 4-formylbenzoic acid, NH<sub>4</sub>OAc, DMF, 100 °C, 7 h, 80%; (b) appropriate secondary or primary diamines, HBTU, DIPEA, DMF, 0 °C to rt, overnight, 69-85%%; (c) 4 N HCl/dioxane, DCM, 0 °C to rt, 6 h, 69-81%;



#### 4. Summary

The novel PARP1 inhibitor **1** was systematically optimized through incremental improvement, and results-based optimization. Starting with the identification of primary amides as an improvement to the ester moiety leading to several compounds with improved  $IC_{50}$  values including **9** which featured a sub-nanomolar  $IC_{50}$  value. Three other sub-nanomolar PARP1 inhibitors, **14**, **15**, and **16**, were identified by changing the linker to aminomethylazetidine. Due to the formation of a new ionic interaction with Glu763 activity was highly conserved when removing pyrimidine, which includes **29** as another sub-nanomolar inhibitor. Other aspects of **1** were addressed such as chemical stability and solubility as well. Changing the linker from piperazine to aminomethylazetidine proved useful in not only maintaining sub-nanomolar  $IC_{50}$  values for each of the three analogues, but also increasing both stability and solubility for the series. Finally, in order to drastically increase solubility and stability the compound was shortened by removing the pyrimidine. Surprisingly, the activity in these compounds were on par with the lead compounds from the pyrimidine series. As expected, these compounds improved solubility and stability by a significant margin. These results are explained well with binding models showcasing specific interactions that lead to stronger inhibition.

## 5. EXPERIMENTAL

### 5.1. Chemical Synthesis

*Materials and Instrumentation.* All the solvents and reagents were purchased and used without further purification. Qualitative analysis of reactions was performed by thin-layer chromatography (TLC) with silica gel G as the adsorbent (250  $\mu\text{m}$ ) on aluminum backed plates (Agela Technologies & Silicycle Inc.) and ultraviolet light at 254 or 365 nm for visualization purposes. NMR experiments were performed using a Bruker 400 Ultrashield spectrometer ( $^1\text{H}$  at 400 MHz and  $^{13}\text{C}$  at 101 MHz) equipped with a z axis gradient probe.  $^1\text{H}$  NMR chemical shifts were reported downfield from tetramethylsilane (TMS, as an internal standard) in parts per million ( $\delta$  ppm) for all the compounds. Column chromatography purifications were performed using silica gel (40–63  $\mu\text{m}$ ) purchased from SiliCycle Inc. (Quebec City, Canada), and flash chromatography was conducted using Reveleris X2 flash chromatography system (BUCHI Corporation, New Castle, DE). Mass analysis of all target compounds was performed on an Agilent 1260 infinity series liquid chromatography (LC) system connected with an Agilent 6120 quadrupole mass spectrometer (MS). Purity analysis of target compounds was carried out using Agilent 1260 infinity series high-performance liquid chromatography (HPLC) system (Column: ZRBAX Eclipse Plus C18, 3.5  $\mu\text{m}$ , 4.6 mm  $\times$  100 mm, and the runs were monitored at 254 nm; Mobile phase: Methanol and water (0.1% formic acid)). High-resolution mass spectroscopy (HRMS) analysis for compounds in the invention were assayed on a Waters Xevo G2-XS Q-ToF mass spectrometer equipped with H-Class UPLC inlet and LockSpray electrospray ionization (ESI).

*Method A: General procedure for coupling reaction of amines and substituted 2-chloropyrimidines.* Appropriate piperazine salt (1 equiv) was dissolved in mixture of dioxane/DMF (8:2) in a reaction vial (with 5-10 mL volume capacity), subsequently *N,N*-diisopropylethylamine (3 equiv) and appropriate 2-chloropyrimidine (1 equiv). The reaction mixture vial was irradiated under microwave condition (160 °C, Biotage Initiator+) for 40 min. After complete consumption of starting compounds, the dioxane was removed under reduced pressure and resulting residue was diluted by adding cold water to affect the precipitation of solid product. The resulting solid was filtered off, washed with cold water and hexanes, and dried in vacuo. Further, the crude product was purified by flash chromatography (silica gel column) using methanol/dichloromethane (0/100% to 15/85%) gradient to furnish pure products.

*Method B: General procedure for the amide coupling reaction.* *N,N*-Diisopropylethylamine (3 equiv) and *O*-(benzotriazol-1-yl)-*N,N,N',N'*-tetramethyluronium hexafluorophosphate (HBTU) (1.1 equiv) was added at 0 °C to a stirred solution of the appropriate carboxylic acid (1 equiv) in *N,N*-dimethylformamide (DMF), and the reaction was stirred for 30 min at the same temperature. Subsequently, the appropriate amine (1.1 equiv) was added as such or by dissolving in minimum volume of DMF to the reaction mixture, and the reaction was stirred at room temperature for overnight. The reaction mixture was then diluted with cold water and sat. aqueous NaHCO<sub>3</sub>, filtered off the precipitation, and solid was washed with water, hexanes, and dried under vacuo. The resulting crude coupled products were purified by flash chromatography using gradient DCM and methanol combinations as the mobile phase,

wherein the concentration of methanol in dichloromethane was varied from 1 to 15% based on the nature of product to be purified.

*Method C: General procedure for the deprotection of piperazines.* To a solution of appropriate *N*-boc piperazine (1.0 eq) in dioxane, concentrated HCl was added drop wise, and the reaction was stirred for six hours at room temperature. The solvent was subsequently evaporated under vacuum and the solid thus obtained was washed with methanol to obtain piperazinium chloride salts in quantitative yields and used as such without further purification for subsequent synthesis.

**5.1.1.** *2-(4-(4-(5-Ethynylpyrimidin-2-yl)piperazine-1-carbonyl)phenyl)-1H-benzo[d]imidazole-4-carboxamide (2).* **2** was synthesized according to the method A using **17** (150 mg, 0.39 mmol), *N,N*-diisopropylethylamine (150 mg, 204  $\mu$ L, 1.17 mmol) and 2-chloro-5-ethynylpyrimidine (57 mg, 0.41 mmol) and was obtained as a cream color solid (55 mg, 31% yield). Mp >300  $^{\circ}$ C (decomposes at this temperature);  $^1$ H NMR (400 MHz, DMSO-*d*<sub>6</sub>)  $\delta$  13.58 (br s, 1H), 9.39 (s, 1H), 8.53 (s, 2H), 8.34 (d, *J* = 8.1 Hz, 2H), 7.86 (d, *J* = 7.2 Hz, 1H), 7.78 (s, 1H), 7.76 (d, *J* = 7.9 Hz, 1H), 7.66 (d, *J* = 8.3 Hz, 2H), 7.34 (t, *J* = 7.7 Hz, 1H), 4.33 (s, 1H), 4.00 – 3.80 (m, 4H), 3.79 – 3.67 (m, 2H), 3.58 – 3.43 (m, 2H);  $^{13}$ C NMR (101 MHz, DMSO)  $\delta$  169.16, 166.84, 160.97, 159.68, 152.23, 141.27, 137.64, 136.84, 131.22, 128.32, 127.42, 123.24, 122.68,

**5.1.2.** *2-(4-(4-(5-(Azetidine-1-carbonyl)pyrimidin-2-yl)piperazine-1-carbonyl)phenyl)-1H-benzo-[d]imidazole-4-carboxamide (3).* **3** was synthesized according to the method B using **26** (100 mg, 0.21 mmol), HBTU (96 mg, 0.25 mmol), *N,N*-diisopropylethylamine (109  $\mu$ L, 0.63 mmol), and azetidine (13 mg, 0.23 mmol) and was obtained as a beige

solid (40 mg, 37% yield). Mp 296 – 298 °C; <sup>1</sup>H NMR (400 MHz, DMSO-*d*<sub>6</sub>) δ 13.68 (br s, 1H), 9.23 (s, 1H), 8.64 (s, 2H), 8.35 (d, *J* = 8.0 Hz, 2H), 7.90 (d, *J* = 7.8 Hz, 1H), 7.86 – 7.76 (m, 2H), 7.69 (d, *J* = 7.7 Hz, 2H), 7.40 (t, *J* = 7.6 Hz, 1H), 4.44 – 4.31 (m, 2H), 4.08 – 3.64 (m, 8H), 3.58 – 3.43 (m, 2H), 2.32 – 2.21 (m, 1H); <sup>13</sup>C NMR (101 MHz, DMSO-*d*<sub>6</sub>) δ 169.02, 166.69, 166.10, 161.40, 158.40, 151.48, 138.23, 135.97, 129.86, 128.33, 127.84, 123.77, 123.45, 122.75, 116.24, 116.04, 53.32, 49.04, 47.27, 44.07, 43.52, 41.87, 16.06; LC-MS (ESI): *m/z*, 511.2 ([M+H]<sup>+</sup> calcd. for C<sub>27</sub>H<sub>26</sub>N<sub>8</sub>O<sub>3</sub>, 511.2); HPLC purity: 94.5% (*t*<sub>R</sub> = 1.02 min).

**5.1.3.**            *2-(4-(4-(5-((2,2,2-trifluoroethyl)carbamoyl)pyrimidin-2-yl)piperazine-1-carbonyl)phenyl)-1H-benzo[d]imidazole-4-carboxamide (4)*. **4** was synthesized according to the method B using **26** (100 mg, 0.21 mmol), HBTU (96 mg, 0.25 mmol), *N,N*-diisopropylethylamine (109 μL, 0.63 mmol), and 2,2,2-trifluoroethylamine (31 mg, 0.32 mmol) and was obtained as a yellow solid (50 mg, 43% yield). Mp 293 – 295 °C; <sup>1</sup>H NMR (400 MHz, DMSO-*d*<sub>6</sub>) δ 13.55 (s, 1H), 9.34 (s, 1H), 9.00 (t, *J* = 6.2 Hz, 1H), 8.85 (s, 2H), 8.34 (d, *J* = 8.1 Hz, 2H), 7.90 (d, *J* = 7.6 Hz, 1H), 7.84 (s, 1H), 7.78 (d, *J* = 8.0 Hz, 1H), 7.69 (d, *J* = 8.1 Hz, 2H), 7.38 (t, *J* = 7.8 Hz, 1H), 4.15 – 4.04 (m, 2H), 4.03 – 3.85 (m, 4H), 3.82 – 3.69 (m, 2H), 3.59 – 3.45 (m, 2H), 3.17 (d, *J* = 5.2 Hz, 3H); <sup>13</sup>C NMR (101 MHz, DMSO-*d*<sub>6</sub>) δ 169.06, 166.53, 164.63, 161.97, 158.43, 151.57, 141.88, 137.91, 135.84, 130.59, 128.41, 127.43, 125.25 (d, *J* = 279.5 Hz), 123.60, 123.11, 123.08, 115.82, 115.64, 55.38, 47.25, 44.13, 43.71, 41.88; LC-MS (ESI): *m/z*, 553.2 ([M+H]<sup>+</sup> calcd. for C<sub>26</sub>H<sub>23</sub>F<sub>3</sub>N<sub>8</sub>O<sub>3</sub>, 553.2); HPLC purity: 100% (*t*<sub>R</sub> = 0.99 min). calcd. for C<sub>29</sub>H<sub>28</sub>N<sub>8</sub>O<sub>3</sub>, 537.2); HPLC purity: 94.7% (*t*<sub>R</sub> = 1.30 min).

**5.1.4.** *2-(4-(4-(5-(Cyclopropylcarbamoyl)pyrimidin-2-yl)piperazine-1-carbonyl)phenyl)-1H-benzo-[d]imidazole-4-carboxamide (5)*. **5** was synthesized according to the method B using **26** (150 mg, 0.32 mmol), HBTU (146 mg, 0.38 mmol), *N,N*-diisopropylethylamine (166  $\mu$ L, 0.96 mmol), and cyclopropylamine (20 mg, 0.35 mmol) and was obtained as a beige solid (43 mg, 39% yield). Mp 295 – 297  $^{\circ}$ C;  $^1$ H NMR (400 MHz, DMSO- $d_6$ )  $\delta$  13.54 (s, 1H), 9.34 (s, 1H), 8.77 (s, 2H), 8.36 (d,  $J$  = 5.9 Hz, 1H), 8.33 (d,  $J$  = 8.2 Hz, 2H), 7.90 (d,  $J$  = 7.5 Hz, 1H), 7.83 (s, 1H), 7.77 (d,  $J$  = 7.9 Hz, 1H), 7.68 (d,  $J$  = 8.1 Hz, 2H), 7.38 (t,  $J$  = 7.8 Hz, 1H), 4.02 – 3.84 (m, 4H), 3.82 – 3.68 (m, 2H), 3.58 – 3.45 (m, 2H), 2.83 – 2.75 (m, 1H), 0.73 – 0.66 (m, 2H), 0.58 – 0.51 (m, 2H);  $^{13}$ C NMR (101 MHz, DMSO- $d_6$ )  $\delta$  169.07, 166.56, 165.16, 161.85, 158.03, 151.58, 141.89, 137.93, 135.84, 130.59, 128.41, 127.44, 123.62, 123.13, 123.08, 116.96, 115.65, 47.25, 44.04, 43.64, 41.88, 23.19, 6.25; LC-MS (ESI):  $m/z$ , 511.2 ( $[M+H]^+$  calcd. for  $C_{27}H_{26}N_8O_3$ , 511.2); HPLC purity: 95.6% ( $t_R$  = 1.11 min).

**5.1.5.** *2-(4-(4-(5-(bicyclo[1.1.1]pentan-1-ylcarbamoyl)pyrimidin-2-yl)piperazine-1-carbonyl)-phenyl)-1H-benzo[d]imidazole-4-carboxamide (6)*. **6** was synthesized according to the method B using **26** (120 mg, 0.25 mmol), HBTU (111 mg, 0.29 mmol), *N,N*-diisopropylethylamine (125  $\mu$ L, 0.72 mmol), and bicyclo[1.1.1]pentan-1-amine hydrochloride (33 mg, 0.28 mmol) and was obtained as a pale yellow solid (55 mg, 32% yield). Mp 286 – 288  $^{\circ}$ C;  $^1$ H NMR (400 MHz, DMSO- $d_6$ )  $\delta$  13.55 (s, 1H), 9.34 (s, 1H), 8.87 (s, 1H), 8.78 (s, 2H), 8.34 (d,  $J$  = 7.3 Hz, 2H), 7.90 (d,  $J$  = 7.6 Hz, 1H), 7.84 (s, 1H), 7.78 (d,  $J$  = 7.5 Hz, 1H), 7.68 (d,  $J$  = 8.1 Hz, 2H), 7.39 (t,  $J$  = 7.0 Hz, 1H), 4.03 – 3.84 (m, 4H), 3.81 – 3.69 (m, 2H), 3.58 – 3.44 (m, 2H), 2.46 (s, 1H), 2.08 (s, 6H);  $^{13}$ C NMR (101 MHz, DMSO- $d_6$ )  $\delta$  169.07, 166.56, 164.14, 161.83, 158.14, 151.58, 141.89, 137.94,

135.85, 130.60, 128.41, 127.44, 123.62, 123.12, 123.09, 116.90, 115.65, 52.92, 49.42, 47.41, 44.17, 43.66, 41.98, 25.17; LC-MS (ESI):  $m/z$ , 537.3 ( $[M+H]^+$ )

**5.1.6.** *2-(4-(4-(5-(oxetan-3-ylcarbamoyl)pyrimidin-2-yl)piperazine-1-carbonyl)phenyl)-1H-benzo-[d]imidazole-4-carboxamide (7)*. **7** was synthesized according to the method B using **26** (100 mg, 0.21 mmol), HBTU (96 mg, 0.25 mmol), *N,N*-diisopropylethylamine (109  $\mu$ L, 0.63 mmol), and oxetan-3-amine (17 mg, 0.23 mmol) and was obtained as a white solid (36 mg, 33% yield). Mp  $>300$  °C (decomposes at this temperature);  $^1\text{H}$  NMR (400 MHz, DMSO- $d_6$ )  $\delta$  13.55 (s, 1H), 9.34 (s, 1H), 9.00 (d,  $J = 6.5$  Hz, 1H), 8.84 (s, 2H), 8.34 (d,  $J = 8.1$  Hz, 2H), 7.90 (d,  $J = 7.1$  Hz, 1H), 7.84 (s, 1H), 7.78 (d,  $J = 7.9$  Hz, 1H), 7.69 (d,  $J = 7.9$  Hz, 2H), 7.39 (t,  $J = 7.7$  Hz, 1H), 5.06 – 4.94 (m, 1H), 4.78 (t,  $J = 6.8$  Hz, 2H), 4.57 (t,  $J = 6.4$  Hz, 2H), 4.05 – 3.84 (m, 4H), 3.82 – 3.70 (m, 2H), 3.58 – 3.44 (m, 2H);  $^{13}\text{C}$  NMR (101 MHz, DMSO- $d_6$ )  $\delta$  169.08, 166.56, 163.67, 161.91, 158.28, 151.58, 141.89, 137.93, 135.85, 130.60, 128.41, 127.44, 123.62, 123.13, 123.08, 116.44, 115.65, 77.44, 47.21, 44.78, 44.11, 43.71, 41.98; LC-MS (ESI):  $m/z$ , 527.2 ( $[M+H]^+$ ) calcd. for  $\text{C}_{27}\text{H}_{26}\text{N}_8\text{O}_4$ , 527.2); HPLC purity: 100% ( $t_R = 0.84$  min).

**5.1.7.** *2-(4-(4-(4-(bicyclo[1.1.1]pentan-1-ylcarbamoyl)pyrimidin-2-yl)piperazine-1-carbonyl)-phenyl)-1H-benzo[d]imidazole-4-carboxamide (8)*. **8** was synthesized according to the method A using **17** (150 mg, 0.39 mmol), *N,N*-diisopropylethylamine (204  $\mu$ L, 1.17 mmol) and *N*-(bicyclo[1.1.1]pentan-1-yl)-2-chloropyrimidine-4-carboxamide (96 mg, 0.43 mmol) and was obtained as a white solid (58 mg, 28% yield). Mp 280 – 282 °C;  $^1\text{H}$  NMR (400 MHz, DMSO- $d_6$ )  $\delta$  13.54 (s, 1H), 9.34 (s, 1H), 9.10 (s, 1H), 8.60 (d,  $J = 4.8$  Hz, 1H), 8.34 (d,  $J = 8.2$  Hz, 2H), 7.90 (d,  $J = 7.6$  Hz, 1H), 7.83 (s,

1H), 7.78 (d,  $J = 8.1$  Hz, 1H), 7.69 (d,  $J = 8.2$  Hz, 2H), 7.39 (t,  $J = 7.7$  Hz, 1H), 7.13 (d,  $J = 4.9$  Hz, 1H), 4.05 – 3.85 (m, 4H), 3.82 – 3.71 (m, 2H), 3.57 – 3.44 (m, 2H), 2.47 (s, 1H), 2.12 (s, 6H);  $^{13}\text{C}$  NMR (101 MHz, DMSO- $d_6$ )  $\delta$  169.07, 166.60, 163.95, 161.14, 160.79, 158.15, 151.62, 141.91, 138.01, 135.90, 130.58, 128.32, 127.48, 123.58, 123.07, 115.68, 107.19, 53.00, 49.17, 47.46, 44.15, 43.70, 42.01, 25.15; LC-MS (ESI):  $m/z$ , 537.3 ( $[\text{M}+\text{H}]^+$  calcd. for  $\text{C}_{29}\text{H}_{28}\text{N}_8\text{O}_3$ , 537.2); HPLC purity: 94.7% ( $t_{\text{R}} = 1.30$  min).

### 5.1.8.

*[4-(cyclopropylcarbamoyl)pyrimidin-2-yl]piperazine-1-carbonyl*phenyl)-1H-1,3-benzodiazole -4-carboxamide (**9**). **9** was synthesized according to the method A using **17** (150 mg, 0.39 mmol), *N,N*-diisopropylethylamine (204  $\mu\text{L}$ , 1.17 mmol) and 2-chloro-*N*-cyclopropylpyrimidine-4-carboxamide (85 mg, 0.43 mmol) and was obtained as a white solid (58 mg, 31% yield). Mp 280 – 282  $^{\circ}\text{C}$ ;  $^1\text{H}$  NMR (400 MHz, DMSO- $d_6$ )  $\delta$  13.54 (s, 1H), 9.34 (s, 1H), 9.10 (s, 1H), 8.60 (d,  $J = 4.8$  Hz, 1H), 8.34 (d,  $J = 8.2$  Hz, 2H), 7.90 (d,  $J = 7.6$  Hz, 1H), 7.83 (s, 1H), 7.78 (d,  $J = 8.1$  Hz, 1H), 7.69 (d,  $J = 8.2$  Hz, 2H), 7.39 (t,  $J = 7.7$  Hz, 1H), 7.13 (d,  $J = 4.9$  Hz, 1H), 4.05 – 3.85 (m, 4H), 3.82 – 3.71 (m, 2H), 3.57 – 3.44 (m, 2H), 2.47 (s, 1H), 2.12 (s, 6H);  $^{13}\text{C}$  NMR (101 MHz, DMSO- $d_6$ )  $\delta$  169.07, 166.60, 163.95, 161.14, 160.79, 158.15, 151.62, 141.91, 138.01, 135.90, 130.58, 128.32, 127.48, 123.58, 123.07, 115.68, 107.19, 53.00, 49.17, 47.46, 44.15, 43.70, 42.01, 25.15; LC-MS (ESI):  $m/z$ , 537.3 ( $[\text{M}+\text{H}]^+$  calcd. for  $\text{C}_{29}\text{H}_{28}\text{N}_8\text{O}_3$ , 537.2); HPLC purity: 94.7% ( $t_{\text{R}} = 1.30$  min).

**5.1.9.** *2-(4-(4-(5-(bicyclo[1.1.1]pentan-1-ylcarbamoyl)pyrimidin-2-yl)piperazine-1-carbonyl)-phenyl)-6-fluoro-1H-benzo[d]imidazole-4-carboxamide* (**10**). **10** was



synthesized according to the method A using **18** (100 mg, 0.26 mmol), *N,N*-diisopropylethylamine (136  $\mu$ L, 0.78 mmol) and *N*-(bicyclo[1.1.1]pentan-1-yl)-2-chloropyrimidine-5-carboxamide (65 mg, 0.29 mmol) and was obtained as a beige solid (50 mg, 35% yield). Mp 244 – 246  $^{\circ}$ C;  $^1$ H NMR (400 MHz, DMSO-*d*<sub>6</sub>)  $\delta$  13.70 (s, 1H), 9.30 (s, 1H), 8.88 (s, 1H), 8.78 (s, 2H), 8.33 (d, *J* = 7.7 Hz, 2H), 8.04 (s, 1H), 7.68 (d, *J* = 7.6 Hz, 2H), 7.62 (d, *J* = 9.6 Hz, 2H), 4.02 – 3.83 (m, 4H), 3.82 – 3.70 (m, 2H), 3.57 – 3.45 (m, 2H), 2.46 (s, 1H), 2.08 (s, 6H); LC-MS (ESI): *m/z*, 555.2 ([M+H]<sup>+</sup> calcd. for C<sub>29</sub>H<sub>27</sub>FN<sub>8</sub>O<sub>3</sub>, 555.2); HPLC purity: 95.8% (*t*<sub>R</sub> = 2.08 min).

**5.1.10.** *2-(4-(4-(4-(bicyclo[1.1.1]pentan-1-yl)carbamoyl)pyrimidin-2-yl)piperazine-1-carbonyl)-phenyl)-6-fluoro-1H-benzo[d]imidazole-4-carboxamide (11). **11** was synthesized according to the method A using **18** (100 mg, 0.26 mmol), *N,N*-diisopropylethylamine (136  $\mu$ L, 0.78 mmol) and *N*-(bicyclo[1.1.1]pentan-1-yl)-2-chloropyrimidine-4-carboxamide (65 mg, 0.29 mmol) and was obtained as a pale yellow solid (47 mg, 33% yield). Mp 247 – 249  $^{\circ}$ C;  $^1$ H NMR (400 MHz, DMSO-*d*<sub>6</sub>)  $\delta$  13.70 (s, 1H), 9.30 (s, 1H), 9.11 (s, 1H), 8.60 (d, *J* = 5.2 Hz, 1H), 8.33 (d, *J* = 8.1 Hz, 2H), 8.05 (s, 1H), 7.69 (d, *J* = 7.9 Hz, 2H), 7.62 (d, *J* = 9.1 Hz, 2H), 7.13 (d, *J* = 4.7 Hz, 1H), 4.09 – 3.83 (m, 4H), 3.82 – 3.68 (m, 2H), 3.56 – 3.41 (m, 2H), 2.47 (s, 1H), 2.11 (s, 6H); LC-MS (ESI): *m/z*, 555.3 ([M+H]<sup>+</sup> calcd. for C<sub>29</sub>H<sub>27</sub>FN<sub>8</sub>O<sub>3</sub>, 555.2); HPLC purity: 97.5% (*t*<sub>R</sub> = 1.03 min).*

**5.1.11.** *2-(4-(4-(5-(cyclopropylcarbamoyl)pyrimidin-2-yl)piperazine-1-carbonyl)phenyl)-6-fluoro-1H-benzo[d]imidazole-4-carboxamide (12).* **12** was synthesized according to the method A using **18** (100 mg, 0.26 mmol), *N,N*-diisopropylethylamine (136  $\mu$ L, 0.78 mmol) and 2-chloro-*N*-cyclopropylpyrimidine-5-carboxamide (57 mg, 0.29 mmol) and

obtained as a pale yellow solid (48 mg, 35% yield). Mp >300 °C (decomposes at this temperature); <sup>1</sup>H NMR (400 MHz, DMSO-*d*<sub>6</sub>) δ 13.69 (s, 1H), 9.29 (s, 1H), 8.77 (s, 2H), 8.37 (d, *J* = 3.4 Hz, 1H), 8.33 (d, *J* = 7.9 Hz, 2H), 8.04 (s, 1H), 7.68 (d, *J* = 8.2 Hz, 2H), 7.62 (d, *J* = 9.0 Hz, 2H), 4.03 – 3.82 (m, 4H), 3.80 – 3.68 (m, 2H), 3.58 – 3.43 (m, 2H), 2.84 – 2.74 (m, 1H), 0.73 – 0.65 (m, 2H), 0.59 – 0.49 (m, 2H); LC-MS (ESI): *m/z*, 529.3 ([M+H]<sup>+</sup> calcd. for C<sub>27</sub>H<sub>25</sub>FN<sub>8</sub>O<sub>3</sub>, 529.2); HPLC purity: 99.3% (*t*<sub>R</sub> = 1.18 min).

**5.1.12**            *6-fluoro-2-(4-(4-(5-(1-methyl-1H-pyrazol-4-yl)pyrimidin-2-yl)piperazine-1-carbonyl)phenyl)-1H-benzo[d]imidazole-4-carboxamide* (**13**). **13** was synthesized according to the method A using **18** (100 mg, 0.26 mmol), *N,N*-diisopropylethylamine (136 μL, 0.78 mmol) and 2-chloro-5-(1-methyl-1H-pyrazol-4-yl)pyrimidine (56 mg, 0.24 mmol) and obtained as a pale yellow solid (50 mg, 37% yield). Mp >300 °C (decomposes at this temperature); <sup>1</sup>H NMR (400 MHz, DMSO-*d*<sub>6</sub>) δ 13.69 (s, 1H), 9.29 (s, 1H), 8.64 (s, 2H), 8.32 (d, *J* = 8.0 Hz, 2H), 8.10 (s, 1H), 8.04 (s, 1H), 7.84 (s, 1H), 7.68 (d, *J* = 8.2 Hz, 2H), 7.62 (d, *J* = 10.3 Hz, 2H), 3.94 – 3.69 (m, 6H), 3.86 (s, 3H), 3.55 – 3.42 (m, 2H); LC-MS (ESI): *m/z*, 526.2 ([M+H]<sup>+</sup> calcd. for C<sub>27</sub>H<sub>24</sub>FN<sub>9</sub>O<sub>2</sub>, 526.2); HPLC purity: 99.4% (*t*<sub>R</sub> = 1.20 min).

**5.1.13.**            *2-{4-[(1-[5-(cyclopropylcarbamoyl)pyrimidin-2-yl]azetidin-3-yl)methyl]carbamoyl}phenyl}-1H-1,3-benzodiazole-4-carboxamide* (**14**). **14** was synthesized according to the method A using **19** (150 mg, 0.33 mmol), *N,N*-diisopropylethylamine (123 mg, 173 μL, 0.99 mmol) and 2-chloro-*N*-cyclopropylpyrimidine-5-carboxamide (78 mg, 0.39 mmol) and was obtained as a cream color solid (62 mg, 35% yield). <sup>1</sup>H NMR (400 MHz, DMSO-*d*<sub>6</sub>) δ 13.58 (s, 1H), 9.32 (s, 1H), 8.87 (t, *J* = 5.5 Hz, 1H), 8.70 (s, 2H), 8.38 – 8.30 (m, 3H), 8.03 (d, *J* = 8.0 Hz, 2H),

7.90 (d,  $J = 7.4$  Hz, 1H), 7.84 (s, 1H), 7.77 (d,  $J = 7.9$  Hz, 1H), 7.38 (t,  $J = 7.7$  Hz, 1H), 4.18 (t,  $J = 8.7$  Hz, 2H), 3.98 – 3.87 (m, 2H), 3.65 – 3.55 (m, 2H), 3.04 – 2.92 (m, 1H), 2.82 – 2.72 (m, 1H), 0.72 – 0.63 (m, 2H), 0.57 – 0.47 (m, 2H). LC-MS (ESI):  $m/z$ , 511.3 ( $[M+H]^+$  calcd. for  $C_{27}H_{26}N_8O_3$ , 511.2); HPLC purity: 95.1% ( $t_R = 1.18$  min).

**5.1.14.** *2-(4-[(1-{5-[(oxetan-3-yl)carbamoyl]pyrimidin-2-yl}azetidin-3-yl)methyl]carbamoyl]phenyl)-1H-1,3-benzodiazole-4-carboxamide (15).* **15** was synthesized according to the method A using **19** (150 mg, 0.33 mmol), *N,N*-diisopropylethylamine (123 mg, 173  $\mu$ L, 0.99 mmol) and 2-chloro-*N*-(oxetan-3-yl)pyrimidine-5-carboxamide (78 mg, 0.39 mmol) and was obtained as a cream color solid (72 mg, 40% yield).  $^1H$  NMR (400 MHz,  $DMSO-d_6$ )  $\delta$  13.55 (s, 1H), 9.32 (s, 1H), 8.95 (d,  $J = 6.4$  Hz, 1H), 8.87 (t,  $J = 5.2$  Hz, 1H), 8.76 (s, 2H), 8.33 (d,  $J = 8.3$  Hz, 2H), 8.03 (d,  $J = 8.3$  Hz, 2H), 7.90 (d,  $J = 7.5$  Hz, 1H), 7.84 (s, 1H), 7.77 (d,  $J = 7.9$  Hz, 1H), 7.39 (t,  $J = 7.8$  Hz, 1H), 5.01 – 4.91 (m, 1H), 4.74 (t,  $J = 6.9$  Hz, 2H), 4.54 (t,  $J = 6.4$  Hz, 2H), 4.20 (t,  $J = 8.6$  Hz, 2H), 3.94 (dd,  $J = 9.1, 5.0$  Hz, 2H), 3.63 – 3.54 (m, 2H), 3.04 – 2.94 (m, 1H); LC-MS (ESI):  $m/z$ , 527.2 ( $[M+H]^+$  calcd. for  $C_{27}H_{26}N_8O_4$ , 527.2); HPLC purity: 99.1% ( $t_R = 1.03$  min).

**5.1.15.** *2-{4-[(1-[4-({bicyclo[1.1.1]pentan-1-yl}carbamoyl)pyrimidin-2-yl]azetidin-3-yl)methyl]carbamoyl]phenyl}-1H-1,3-benzodiazole-4-carboxamide (16).* **16** was synthesized according to the method A using **19** (150 mg, 0.33 mmol), *N,N*-diisopropylethylamine (123 mg, 173  $\mu$ L, 0.99 mmol) and *N*-(bicyclo[1.1.1]pentan-1-yl)-2-chloropyrimidine-4-carboxamide (87 mg, 0.39 mmol) and was obtained as a cream color solid (57 mg, 32% yield).  $^1H$  NMR (400 MHz,  $DMSO-d_6$ )  $\delta$  13.56 (s, 1H), 9.32 (s,

1H), 8.92 (s, 1H), 8.87 (t,  $J = 4.1$  Hz, 1H), 8.54 (d,  $J = 4.6$  Hz, 1H), 8.34 (d,  $J = 8.2$  Hz, 2H), 8.05 (d,  $J = 8.5$  Hz, 2H), 7.90 (d,  $J = 7.2$  Hz, 1H), 7.85 (s, 1H), 7.78 (d,  $J = 7.7$  Hz, 1H), 7.39 (t,  $J = 7.8$  Hz, 1H), 7.09 (d,  $J = 5.1$  Hz, 1H), 4.20 (t,  $J = 8.4$  Hz, 2H), 3.98 – 3.88 (m, 2H), 3.65 – 3.56 (m, 2H), 3.05 – 2.93 (m, 1H), 2.51 (s, 6H), 2.46 (s, 1H); LC-MS (ESI):  $m/z$ , 537.3 ( $[M+H]^+$  calcd. for  $C_{29}H_{28}N_8O_3$ , 537.2); HPLC purity: 95.7% ( $t_R = 1.65$  min).

**5.1.16.** *4-(4-(4-Carbamoyl-1H-benzo[d]imidazol-2-yl)benzoyl)piperazin-1-ium chloride (17)*. Step 1. The amide coupling reaction was performed according to the method B using **24** (500 mg, 1.78 mmol), HBTU (809 mg, 2.13 mmol), *N,N*-diisopropylethylamine (619  $\mu$ L, 3.56 mmol), and *N*-boc piperazine (364 mg, 1.96 mmol) to obtain the compound as a beige solid (685 mg, 85%) after flash chromatography purification.

Step 2. To a stirred solution of amide (680 mg, 1.51 mmol) in dichloromethane (20.0 mL) at 0 °C, was added solution of 4N HCl/Dioxane (10.0 mL) slowly dropwise. The reaction mixture was allowed to stir at room temperature for 6h. After completion of the reaction, solvent was removed under reduced pressure and the resulting residue was triturated with methanol: diethyl ether (1:9) to affect precipitation of the product. Filtered off the solid and dried under vacuo to furnish corresponding piperazine hydrochloride salt (510 mg, 87%) as beige solid. The salt was used for subsequent reactions without further purification.  $^1H$  NMR (400 MHz, DMSO- $d_6$ )  $\delta$  9.68 (br s, 2H), 8.99 (s, 1H), 8.43 (d,  $J = 8.2$  Hz, 2H), 7.95 (d,  $J = 7.4$  Hz, 1H), 7.90 (d,  $J = 8.0$  Hz, 1H), 7.86 (s, 1H), 7.73 (d,  $J = 8.2$  Hz, 2H), 7.49 (t,  $J = 7.8$  Hz, 1H), 6.02 (br s, 2H), 4.07 – 3.46 (m, 4H), 3.29 – 3.03 (m, 4H); LC-MS (ESI):  $m/z$ , 351.2 ( $[M]^+$  calcd. for  $C_{19}H_{21}N_5O_2^+$ , 351.2).

**5.1.17.** *4-(4-(4-carbamoyl-6-fluoro-1H-benzo[d]imidazol-2-yl)benzoyl)piperazinium dihydrochloride (18)*. **18** was synthesized from **25** (600 mg, 1.28 mmol) using a procedure similar to that described for the synthesis of **17** and was obtained as pale brown solid (458 mg, 81%). <sup>1</sup>H NMR (400 MHz, DMSO-*d*<sub>6</sub>) δ 9.40 (br s, 1H), 9.20 (s, 1H), 8.36 (d, *J* = 8.0 Hz, 2H), 8.02 (s, 1H), 7.69 (d, *J* = 8.0 Hz, 2H), 7.66 – 7.60 (m, 2H), 3.47 – 3.43 (m, 8H), 3.28 – 3.05 (m, 2H). LC-MS (ESI): *m/z*, 368.2 ([M]<sup>+</sup> calcd. for C<sub>19</sub>H<sub>19</sub>FN<sub>5</sub>O<sub>2</sub><sup>+</sup>, 368.2).

**5.1.18.**

*2-(4-{[(azetidin-1-ium-3-yl)methyl]carbamoyl}phenyl)-4-carbamoyl-2,3-dihydro-1H-1,3-benzodiazol-1-ium dichloride (19)*. Step 1. The amide coupling reaction was performed according to the method B using **24** (500 mg, 1.78 mmol), HBTU (809 mg, 2.13 mmol), *N,N*-diisopropylethylamine (459 mg, 619 μL, 3.56 mmol), and *tert*-butyl 3-(aminomethyl)azetidine-1-carboxylate (365 mg, 357 μL, 1.96 mmol) to obtain *tert*-butyl 3-((4-(4-carbamoyl-1H-benzo[d]imidazol-2-yl)benzamido)methyl)azetidine-1-carboxylate as beige solid (690 mg, 86%) after flash chromatography purification.

Step 2. Boc deprotection was performed following the procedure for the synthesis of compound **17** using *tert*-butyl 3-((4-(4-carbamoyl-1H-benzo[d]imidazol-2-yl)benzamido)methyl)azetidine-1-carboxylate (690 mg, 1.54 mmol) from step 1 in dichloromethane (20 mL), and HCl (10 mL, 4 N in 1,4-dioxane), and the obtained compound **19** (507 mg, 73%) was used in the next step without further purification. <sup>1</sup>H NMR (400 MHz, DMSO-*d*<sub>6</sub>) 4.03 – 3.92 (m, 2H), 3.88 – 3.77 (m, 4H), 3.53 (t, *J* = 5.8 Hz, 2H), 3.11 – 2.99 (m, 1H), δ 9.40 (br s, 1H), 9.20 (s, 1H), 8.36 (d, *J* = 8.0 Hz, 2H),

8.02 (s, 1H), 7.69 (d,  $J = 8.0$  Hz, 2H), 7.66 – 7.60 (m, 2H); LC-MS (ESI):  $m/z$ , 5351.2 ([M]<sup>+</sup> calcd. for C<sub>19</sub>H<sub>21</sub>N<sub>5</sub>O<sub>2</sub><sup>2+</sup>, 351.2); HPLC purity: 98.2% ( $t_R = 0.82$  min).

#### 5.1.19.

*4-carbamoyl-2-(4-{2,6-diazaspiro[3.3]heptan-6-ium-2-carbonyl}phenyl)-1H-1,3-benzodiazol-1-ium dichloride (20)*. Step 1. The amide coupling reaction was performed according to the method B using **24** (250 mg, 0.89 mmol), HBTU (406 mg, 1.07 mmol), *N,N*-diisopropylethylamine (345 mg, 465  $\mu$ L, 2.67 mmol), and *tert*-Butyl 2,6-diazaspiro[3.3]heptane-2-carboxylate (194 mg, 0.98 mmol) to obtain *tert*-butyl 6-(4-(4-carbamoyl-1*H*-benzo[*d*]imidazol-2-yl)benzoyl)-2,6-diazaspiro[3.3]heptane-2-carboxylate as beige solid (248 mg, 60%) after flash chromatography purification.

Step 2. Boc deprotection was performed following the procedure for the synthesis of compound **17** using *tert*-butyl 6-(4-(4-carbamoyl-1*H*-benzo[*d*]imidazol-2-yl)benzoyl)-2,6-diazaspiro[3.3]heptane-2-carboxylate (248 mg, 0.53 mmol) from step 1 in dichloromethane (10 mL), and HCl (5 mL, 4 N in 1,4-dioxane), and the obtained compound **20** (150 mg, 65%) was used in the next step without further purification. <sup>1</sup>H NMR (400 MHz, DMSO-*d*<sub>6</sub>):  $\delta$  2.91 (4H, d,  $J = 7.4$  Hz), 3.47 (4H, d,  $J = 13.7$  Hz), 7.51 (1H, dd,  $J = 8.1, 8.0$  Hz), 7.78 (1H, dd,  $J = 8.0, 2.0$  Hz), 7.86 (1H, dd,  $J = 8.1, 2.0$  Hz), 8.02-8.09 (4H, 8.06 (ddd,  $J = 8.8, 1.5, 0.4$  Hz), 8.05 (ddd,  $J = 8.8, 1.6, 0.4$  Hz) LC-MS (ESI):  $m/z$ , 362.2 ([M]<sup>+</sup> calcd. for C<sub>20</sub>H<sub>21</sub>N<sub>5</sub>O<sub>2</sub><sup>2+</sup>, 362.2); HPLC purity: 95.4% ( $t_R = 0.79$  min).

#### 5.1.20.

*4-carbamoyl-2-(4-{[(piperidin-1-ium-4-yl)methyl]carbamoyl}phenyl)-1H-1,3-benzodiazol-1-ium dichloride (20)*

*l*-*l*-ium dichloride (**21**). Step 1. The amide coupling reaction was performed according to the method B using **24** (250 mg, 0.89 mmol), HBTU (406 mg, 1.07 mmol), *N,N*-diisopropylethylamine (345 mg, 465  $\mu$ L, 2.67 mmol), and *tert*-butyl 4-(aminomethyl)piperidine-1-carboxylate (365 mg, 357  $\mu$ L, 1.96 mmol) to obtain *tert*-butyl 4-((4-(4-carbamoyl-1*H*-benzo[*d*]imidazol-2-yl)benzamido)methyl)piperidine-1-carboxylate as beige solid (278 mg, 65%) after flash chromatography purification.

Step 2. Boc deprotection was performed following the procedure for the synthesis of compound **17** using *tert*-butyl 4-((4-(4-carbamoyl-1*H*-benzo[*d*]imidazol-2-yl)benzamido)methyl)piperidine-1-carboxylate (278 mg, 0.58 mmol) from step 1 in dichloromethane (10 mL), and HCl (5 mL, 4 N in 1,4-dioxane), and the obtained compound **21** (180 mg, 69%) was used in the next step without further purification.  $^1\text{H}$  NMR (400 MHz, DMSO-*d*<sub>6</sub>)  $\delta$  8.89 – 8.75 (m, 2H), 8.60 – 8.48 (br s, 1H), 8.37 (d, *J* = 8.1 Hz, 2H), 8.06 (d, *J* = 8.3 Hz, 2H), 7.90 (d, *J* = 7.7 Hz, 1H), 7.83 (s, 1H), 7.79 (d, *J* = 7.7 Hz, 1H), 7.39 (t, *J* = 7.7 Hz, 1H), 3.33 – 3.18 (m, 4H), 2.93 – 2.77 (m, 2H), 1.92 – 1.78 (m, 3H), 1.48 – 1.31 (m, 2H); LC-MS (ESI): *m/z*, 379.2 ( $[\text{M}]^+$  calcd. for C<sub>21</sub>H<sub>25</sub>N<sub>5</sub>O<sub>2</sub><sup>2+</sup>, 379.2); HPLC purity: 99.6% (*t*<sub>R</sub> = 0.81 min).

#### 5.1.21.

*4*-carbamoyl-2-(4-{{(3*R*)-pyrrolidin-1-ium-3-yl}carbamoyl}phenyl)-1*H*-1,3-benzodiazol-1-ium dichloride (**22**). Step 1. The amide coupling reaction was performed according to the method B using **24** (250 mg, 0.89 mmol), HBTU (406 mg, 1.07 mmol), *N,N*-diisopropylethylamine (345 mg, 465  $\mu$ L, 2.67 mmol), and (*R*)-*tert*-butyl 3-aminopyrrolidine-1-carboxylate hydrochloride (218 mg, 0.98 mmol) to obtain *tert*-butyl

(R)-3-(4-(4-carbamoyl-1*H*-benzo[*d*]imidazol-2-yl)benzamido)pyrrolidine-1-carboxylate as beige solid (279 mg, 70%) after flash chromatography purification.

Step 2. Boc deprotection was performed following the procedure for the synthesis of compound **17** using *tert*-butyl (R)-3-(4-(4-carbamoyl-1*H*-benzo[*d*]imidazol-2-yl)benzamido)pyrrolidine-1-carboxylate (279 mg, 0.62 mmol) from step 1 in dichloromethane (10 mL), and HCl (5 mL, 4 N in 1,4-dioxane), and the obtained compound **22** (154 mg, 59%) was used in the next step without further purification. <sup>1</sup>H NMR (400 MHz, DMSO-*d*<sub>6</sub>) δ 9.37 – 9.25 (m, 1H), 9.24 – 9.08 (m, 2H), 8.94 (d, *J* = 6.5 Hz, 1H), 8.38 (d, *J* = 8.2 Hz, 2H), 8.12 (d, *J* = 8.2 Hz, 2H), 7.90 (d, *J* = 7.5 Hz, 1H), 7.83 (s, 1H), 7.80 (d, *J* = 7.9 Hz, 1H), 7.40 (t, *J* = 7.7 Hz, 1H), 4.63 – 4.52 (m, 1H), 3.49 – 3.34 (m, 2H), 3.32 – 3.19 (m, 2H), 2.28 – 2.15 (m, 1H), 2.12 – 1.96 (m, 1H); LC-MS (ESI): *m/z*, 351.2 ([*M*]<sup>+</sup> calcd. for C<sub>19</sub>H<sub>21</sub>N<sub>5</sub>O<sub>2</sub><sup>2+</sup>, 351.2); HPLC purity: 97.5% (*t*<sub>R</sub> = 0.82 min)

#### 5.1.22.

*4-carbamoyl-2-(4-{{(3*S*)-pyrrolidin-1-ium-3-yl}carbamoyl}phenyl)-1*H*-1,3-benzodiazol-1-ium dichloride (23)*. Step 1. The amide coupling reaction was performed according to the method A using **24** (250 mg, 0.89 mmol), HBTU (406 mg, 1.07 mmol), *N,N*-diisopropylethylamine (345 mg, 465 μL, 2.67 mmol), and (*S*)-*tert*-butyl 3-aminopyrrolidine-1-carboxylate hydrochloride (218 mg, 0.98 mmol) to obtain *tert*-butyl (*S*)-3-(4-(4-carbamoyl-1*H*-benzo[*d*]imidazol-2-yl)benzamido)pyrrolidine-1-carboxylate as beige solid (286 mg, 72%) after flash chromatography purification.



Step 2. Boc deprotection was performed following the procedure for the synthesis of compound **17** using *tert*-butyl (R)-3-(4-(4-carbamoyl-1*H*-benzo[*d*]imidazol-2-yl)benzamido)pyrrolidine-1-carboxylate (286 mg, 0.64 mmol) from step 1 in dichloromethane (10 mL), and HCl (5 mL, 4 N in 1,4-dioxane), and the obtained compound **23** (143 mg, 53%) was used in the next step without further purification. <sup>1</sup>H NMR (400 MHz, DMSO-*d*<sub>6</sub>) δ 9.61 – 9.48 (m, 1H), 9.46 – 9.34 (m, 1H), 9.13 – 8.99 (m, 2H), 8.41 (d, *J* = 8.3 Hz, 2H), 8.17 (d, *J* = 8.4 Hz, 2H), 7.93 (d, *J* = 7.4 Hz, 1H), 7.90 – 7.80 (m, 2H), 7.46 (t, *J* = 7.8 Hz, 1H), 4.68 – 4.54 (m, 1H), 3.50 – 3.36 (m, 2H), 3.34 – 3.20 (m, 2H), 2.30 – 2.15 (m, 1H), 2.12 – 1.98 (m, 1H); LC-MS (ESI): *m/z*, 351.2 ([M]<sup>+</sup> calcd. for C<sub>19</sub>H<sub>21</sub>N<sub>5</sub>O<sub>2</sub><sup>2+</sup>, 351.2); HPLC purity: 97.6% (*t*<sub>R</sub> = 0.82 min).

**5.1.23.** *4-(4-carbamoyl-1H-benzo[*d*]imidazol-2-yl)benzoic acid (24)*. To a solution of 2,3-diamino benzamide (DAB) (1000 mg, 6.62 mmol) in DMF (10.0 mL), 4-formyl benzoic acid (1090 mg, 7.28 mmol) was added, followed by the subsequent addition of ammonium acetate (770 mg, 9.92 mmol). The mixture was then heated at 60 °C for a period of 6 h after which the solvent was evaporated under vacuum. The resulting solid was washed with methanol and water to obtain **24** as light to dark yellow powder (1600 mg, 86% yield). <sup>1</sup>H NMR (400 MHz, DMSO-*d*<sub>6</sub>) δ 13.65 (s, 1H), 13.25 (br s, 1H), 9.32 (s, 1H), 8.37 (d, *J* = 8.2 Hz, 2H), 8.15 (d, *J* = 8.2 Hz, 2H), 7.94 – 7.74 (m, 3H), 7.40 (t, *J* = 7.8 Hz, 1H). LC-MS (ESI): *m/z*, 282.1 ([M+H]<sup>+</sup> calcd. for C<sub>15</sub>H<sub>11</sub>N<sub>3</sub>O<sub>3</sub>, 282.1).

**5.1.24.** *4-(4-carbamoyl-6-fluoro-1H-benzo[*d*]imidazol-2-yl)benzoic acid (25)*. **25** was synthesized from 2,3-diamino-5-fluorobenzamide (500 mg, 2.95 mmol), 4-formylbenzoic acid (443 mg, 2.95 mmol) and ammonium acetate (341 mg, 4.42 mmol) using a

procedure similar to that described for the synthesis of **24** and was obtained as pale brown solid (710 mg, 80%). <sup>1</sup>H NMR (400 MHz, DMSO-*d*<sub>6</sub>) δ 13.78 (s, 1H), 13.26 (br s, 1H), 9.27 (s, 1H), 8.36 (d, *J* = 8.0 Hz, 2H), 8.14 (d, *J* = 8.2 Hz, 2H), 8.04 (s, 1H), 7.67 – 7.58 (m, 2H); LC-MS (ESI): *m/z*, 300.1 ([M+H]<sup>+</sup> calcd. for C<sub>15</sub>H<sub>10</sub>FN<sub>3</sub>O<sub>3</sub>, 300.1).

**5.1.25.** *2-(4-(4-(4-carbamoyl-1H-benzo[d]imidazol-2-yl)benzoyl)piperazin-1-yl)pyrimidine-5-carboxylic acid (26)*. The piperazine salt **17** (500 mg, 1.29 mmol) was dissolved in mixture of dioxane/DMF (8:2, 10 mL) in a reaction vial (with 5-10 mL volume capacity), subsequently *N,N*-diisopropylethylamine (676 μL, 3.89 mmol) and 2-chloropyrimidine-5-carboxylic acid (205 mg, 1.29 mmol). The reaction mixture vial was irradiated under microwave condition (160 °C, Biotage Initiator+) for 60 min. After complete consumption of starting compounds, the dioxane was removed under reduced pressure and resulting residue was diluted by adding cold water, and adjusted pH to 6 by using 10% HCl to affect the precipitation of solid product. The resulting solid was filtered off, washed with cold water and hexanes, and dried in vacuo to obtain the acid (422 mg, 69%) as a pale brown solid. The acid was used in the next step without further purification. <sup>1</sup>H NMR (400 MHz, DMSO-*d*<sub>6</sub>) δ 13.57 (s, 1H), 12.93 (br s, 1H), 9.33 (br s, 1H), 8.81 (s, 2H), 8.35 (d, *J* = 8.0 Hz, 2H), 7.90 (d, *J* = 7.4 Hz, 1H), 7.84 (s, 1H), 7.79 (d, *J* = 8.0 Hz, 1H), 7.69 (d, *J* = 8.1 Hz, 2H), 7.38 (t, *J* = 7.8 Hz, 1H), 4.09 – 3.86 (m, 4H), 3.84 – 3.68 (m, 2H), 3.63 – 3.47 (m, 2H); LC-MS (ESI): *m/z*, 472.2 ([M+H]<sup>+</sup> calcd. for C<sub>24</sub>H<sub>21</sub>N<sub>7</sub>O<sub>4</sub>, 472.2).

**5.1.26.** *N-(bicyclo[1.1.1]pentan-1-yl)-2-chloropyrimidine-4-carboxamide (27)*. To a solution of 2-chloropyrimidine-4-carboxylic acid (200 mg, 1.26 mmol) in

dichloromethane (5.0 mL), oxalyl chloride (162  $\mu$ L, 1.89 mmol) was added dropwise. A catalytic amount of DMF was added and the reaction mixture was refluxed for two hours. Upon reaction completion, the reaction mixture was concentrated under reduced pressure and obtained residue was re-dissolved in tetrahydrofuran (5.0 mL). Bicyclo[1.1.1]pentan-1-amine hydrochloride (185 mg, 1.51 mmol) was added to the reaction mixture and solution was stirred overnight. Then, the reaction mixture was partitioned between ethyl acetate and water. The organic layer was washed with brine (2 X 5.0 mL) and dried over anhydrous  $\text{Na}_2\text{SO}_4$ . Organic solvent was removed under reduced pressure and formed residue was purified by flash chromatography (silica gel) using ethyl acetate/hexanes (1:19 to 1:3) to obtain compound **27** (191 mg, 68%) as white solid. LC-MS (ESI):  $m/z$ , 223.1 ( $[\text{M}]^+$  calcd. for  $\text{C}_{10}\text{H}_{10}\text{ClN}_3\text{O}$ , 223.1).  $^1\text{H}$  NMR (400 MHz,  $\text{DMSO-}d_6$ ) 9.50 (s, 1H), 9.00 (d,  $J = 4.9$  Hz, 1H), 7.97 (d,  $J = 4.9$  Hz, 1H), 2.50 (s, 6H), 2.47 (s, 1H); LC-MS (ESI):  $m/z$ , 223.1 ( $[\text{M}]^+$  calcd. for  $\text{C}_{10}\text{H}_{10}\text{ClN}_3\text{O}$ , 223.1).

**5.1.27.** *2-chloro-N-cyclopropylpyrimidine-4-carboxamide (28)*. To a solution of 2-chloropyrimidine-4-carboxylic acid (200 mg, 1.26 mmol) in dichloromethane (5.0 mL), oxalyl chloride (162  $\mu$ L, 1.89 mmol) was added dropwise. A catalytic amount of DMF was added and the reaction mixture was refluxed for two hours. Upon reaction completion, the reaction mixture was concentrated under reduced pressure and obtained residue was re-dissolved in tetrahydrofuran (5.0 mL). Cyclopropylamine (86 mg, 105  $\mu$ L, 1.51 mmol) was added to the reaction mixture and solution was stirred overnight. Then, the reaction mixture was partitioned between ethyl acetate and water. The organic layer was washed with brine (2 X 5.0 mL) and dried over anhydrous  $\text{Na}_2\text{SO}_4$ . Organic solvent was removed under reduced pressure and formed residue was purified by flash

chromatography (silica gel) using ethyl acetate/hexanes (1:19 to 1:3) to obtain compound **28** (191 mg, 68%) as white solid. LC-MS (ESI):  $m/z$ , 223.1 ( $[M]^+$  calcd. for  $C_{10}H_{10}ClN_3O$ , 223.1).  $^1H$  NMR (400 MHz,  $DMSO-d_6$ )  $\delta$  9.00 (d,  $J = 4.5$  Hz, 1H), 8.00 (d,  $J = 5.0$  Hz, 1H), 2.97 – 2.88 (m, 1H), 0.76 – 0.66 (m, 4H).

## 5.2. PARP biochemical assay

PARP inhibitor screening, including PARP isoform screening, and  $IC_{50}$  determination were conducted essentially according to previously published chemiluminescence assay protocol at BPS Bioscience, CA.<sup>39,48</sup>

## 5.3. Determination of Aqueous Solubility and Stability

The aqueous solubility and stability of selected compounds was determined using shake flask thermodynamic solubility assay.<sup>47</sup> Each selected compound was dissolved in PBS buffer (pH 4.0 and 7.4) and DMSO at 1 mg/mL and shaken at 750 rpm for 24 h. Then, the solutions were filtered through 0.2  $\mu m$  PTFE (MicroSolv AQ<sup>TM</sup>) syringe filters and analyzed the area under the curve (AUC) using high-performance liquid chromatography (HPLC), along with the standard DMSO solution of compound. Then, determined the solubility of compounds in PBS buffer (pH 4.0 and pH 7.4). Stability was determined by the ratio of AUC for the primary (parent compound) peak over the AUC of all secondary (degradation product) peaks.

## 5.4. Kinase Panel Assay

Select compounds were screened against a panel of 12 kinases (Ser/Thr and tyrosine) at 100 nM concentration at ThermoFisher Scientific (Waltham, MA).

## 5.5. Molecular Modeling

X-ray crystal structure of **1** bound to a full length PARP1 (PDB ID: 6VKO) was selected for docking studies using Glide v. 5.5 (Schrodinger, LLC, New York, NY). The protein structure was refined using Schrodinger's "Protein Preparation Wizard" tool with default parameters. Compound **1** was considered as a reference ligand to create grid for Glide docking. Selected PARP inhibitors were imported in Maestro as mol files and subjected to LigPrep v. 2.3 tool with all variable settings at their default values, including ionization at physiological pH. Prepared PARPi were then docked using SP method available in Glide docking tool according to out published protocols.<sup>39, 48</sup> Default values were chosen, except that the number of poses per ligand were set to 10. Top scoring pose each of the selected PARPi was used to generate graphical representation.

## 6. REFERENCES

- (1) Hottiger, M. O.; Hassa, P. O.; Luscher, B.; Schuler, H.; Koch-Nolte, F. Toward a unified nomenclature for mammalian ADP-ribosyltransferases. *Trends Biochem. Sci.* **2010**, *35*, 208-219.
- (2) Ame, J. C.; Spenlehauer, C.; de Murcia, G. The PARP superfamily. *BioEssays : news and reviews in molecular, cellular and developmental biology* **2004**, *26*, 882-893.
- (3) Yelamos, José & Farres, Jordi & Llacuna, Laura & Ampurdanés, Coral & Martín-Caballero, Juan. (2011). PARP-1 and PARP-2: new players in tumour development. *American journal of cancer research*. 1. 328-346.
- (4) Hassa, P. O.; Hottiger, M. O. The diverse biological roles of mammalian PARPS, a small but powerful family of poly-ADP-ribose polymerases. *Front. Biosci.* **2008**, *13*, 3046-3082.
- (5) Yelamos, J.; Schreiber, V.; Dantzer, F. Toward specific functions of poly(ADP-ribose) polymerase-2. *Trends Mol. Med.* **2008**, *14*, 169-178.
- (6) Tan, E. S.; Krukenberg, K. A.; Mitchison, T. J. Large-scale preparation and characterization of poly(ADP-ribose) and defined length polymers. *Anal. Biochem.* **2012**, *428*, 126-136.
- (7) Burkle, A. Poly(ADP-ribose). The most elaborate metabolite of NAD<sup>+</sup>. *FEBS J.* **2005**, *272*, 4576-4589.
- (8) Schreiber, V.; Dantzer, F.; Ame, J. C.; de Murcia, G. Poly(ADP-ribose): novel functions for an old molecule. *Nat. Rev. Mol. Cell Biol.* **2006**, *7*, 517-528.
- (9) Beneke, S. Regulation of chromatin structure by poly(ADP-ribosylation). *Front. Genet.* **2012**, *3*, 169.
- (10) Caldecott, K. W. XRCC1 and DNA strand break repair. *DNA repair* **2003**, *2*, 955-969.
- (11) Audebert, M.; Salles, B.; Calsou, P. Involvement of poly(ADP-ribose) polymerase-1 and XRCC1/DNA ligase III in an alternative route for DNA double-strand breaks rejoining. *J. Biol. Chem.* **2004**, *279*, 55117-55126.
- (12) Hassa PO, Haenni SS, Elser M, Hottiger MO. Nuclear ADP-ribosylation reactions in mammalian cells: where are we today and where are we going? *Microbiol Mol Biol Rev.* 2006 Sep;70(3):789-829. doi: 10.1128/MMBR.00040-05. PMID: 16959969; PMCID: PMC1594587.
- (13) Tao M, Park CH, Bihovsky R, Wells GJ, Husten J, Ator MA, Hudkins RL. Synthesis and structure-activity relationships of novel poly(ADP-ribose) polymerase-1 inhibitors. *Bioorg Med Chem Lett.* 2006 Feb 15;16(4):938-42. doi: 10.1016/j.bmcl.2005.10.099. Epub 2005 Nov 15. PMID: 16290935.
- (14) Ferraris, D. V. Evolution of poly(ADP-ribose) polymerase-1 (PARP-1) inhibitors. From concept to clinic. *J. Med. Chem.* **2010**, *53*, 4561-4584.
- (15) Liu, X.; Shi, Y.; Guan, R.; Donawho, C.; Luo, Y.; Palma, J.; Zhu, G. D.; Johnson, E. F.; Rodriguez, L. E.; Ghoreishi-Haack, N.; Jarvis, K.; Hradil, V. P.; Colon-Lopez, M.; Cox, B. F.; Klinghofer, V.; Penning, T.; Rosenberg, S. H.; Frost, D.; Giranda, V. L.; Luo, Y. Potentiation of temozolomide cytotoxicity by poly(ADP)ribose polymerase inhibitor ABT-888 requires a conversion of single-stranded DNA damages to double-stranded DNA breaks. *Mol. Cancer Res.* **2008**, *6*, 1621-1629.

- (16) Smith, L. M.; Willmore, E.; Austin, C. A.; Curtin, N. J. The novel poly(ADP-Ribose) polymerase inhibitor, AG14361, sensitizes cells to topoisomerase I poisons by increasing the persistence of DNA strand breaks. *Clin. Cancer Res.* **2005**, *11*, 8449-8457.
- (17) Donawho, C. K.; Luo, Y.; Luo, Y.; Penning, T. D.; Bauch, J. L.; Bouska, J. J.; Bontcheva-Diaz, V. D.; Cox, B. F.; DeWeese, T. L.; Dillehay, L. E.; Ferguson, D. C.; Ghoreishi-Haack, N. S.; Grimm, D. R.; Guan, R.; Han, E. K.; Holley-Shanks, R. R.; Hristov, B.; Idler, K. B.; Jarvis, K.; Johnson, E. F.; Kleinberg, L. R.; Klinghofer, V.; Lasko, L. M.; Liu, X.; Marsh, K. C.; McGonigal, T. P.; Meulbroek, J. A.; Olson, A. M.; Palma, J. P.; Rodriguez, L. E.; Shi, Y.; Stavropoulos, J. A.; Tsurutani, A. C.; Zhu, G. D.; Rosenberg, S. H.; Giranda, V. L.; Frost, D. J. ABT-888, an orally active poly(ADP-ribose) polymerase inhibitor that potentiates DNA-damaging agents in preclinical tumor models. *Clin. Cancer Res.* **2007**, *13*, 2728-2737.
- (18) Wang, L.; Mason, K. A.; Ang, K. K.; Buchholz, T.; Valdecanas, D.; Mathur, A.; Buser-Doepner, C.; Toniatti, C.; Milas, L. MK-4827, a PARP-1/-2 inhibitor, strongly enhances response of human lung and breast cancer xenografts to radiation. *Invest. New Drugs* **2012**, *30*, 2113-2120.
- (19) Senra, J. M.; Telfer, B. A.; Cherry, K. E.; McCrudden, C. M.; Hirst, D. G.; O'Connor, M. J.; Wedge, S. R.; Stratford, I. J. Inhibition of PARP-1 by olaparib (AZD2281) increases the radiosensitivity of a lung tumor xenograft. *Mol. Cancer Ther.* **2011**, *10*, 1949-1958.
- (20) Underhill, C.; Toulmonde, M.; Bonnefoi, H. A review of PARP inhibitors: from bench to bedside. *Ann. Oncol.* **2011**, *22*, 268-279.
- (21) O'Connor, M. J. Targeting the DNA damage response in cancer. *Mol. Cell* **2015**, *60*, 547-560.
- (22) Bryant, H. E.; Schultz, N.; Thomas, H. D.; Parker, K. M.; Flower, D.; Lopez, E.; Kyle, S.; Meuth, M.; Curtin, N. J.; Helleday, T. Specific killing of BRCA2-deficient tumours with inhibitors of poly(ADP-ribose) polymerase. *Nature* **2005**, *434*, 913-917.
- (23) Farmer, H.; McCabe, N.; Lord, C. J.; Tutt, A. N.; Johnson, D. A.; Richardson, T. B.; Santarosa, M.; Dillon, K. J.; Hickson, I.; Knights, C.; Martin, N. M.; Jackson, S. P.; Smith, G. C.; Ashworth, A. Targeting the DNA repair defect in BRCA mutant cells as a therapeutic strategy. *Nature* **2005**, *434*, 917-921.
- (24) Kennedy, R. D.; D'Andrea, A. D. DNA repair pathways in clinical practice: lessons from pediatric cancer susceptibility syndromes. *J. Clin. Oncol.* **2006**, *24*, 3799-3808.
- (25) Cerbinskaite, A.; Mukhopadhyay, A.; Plummer, E. R.; Curtin, N. J.; Edmondson, R. J. Defective homologous recombination in human cancers. *Cancer Treat. Rev.* **2012**, *38*, 89-100.
- (26) Su, J. M.; Thompson, P.; Adesina, A.; Li, X. N.; Kilburn, L.; Onar-Thomas, A.; Kocak, M.; Chyla, B.; McKeegan, E.; Warren, K. E.; Goldman, S.; Pollack, I. F.; Fouladi, M.; Chen, A.; Giranda, V.; Boyett, J.; Kun, L.; Blaney, S. M. A phase I trial of veliparib (ABT-888) and temozolomide in children with recurrent CNS tumors: a pediatric brain tumor consortium report. *Neuro-Oncol* **2014**, *16*, 1661-1668.
- (27) Rajan, A.; Carter, C. A.; Kelly, R. J.; Gutierrez, M.; Kummur, S.; Szabo, E.; Yancey, M. A.; Ji, J.; Mannargudi, B.; Woo, S.; Spencer, S.; Figg, W. D.; Giaccone, G. A phase I combination study of olaparib with cisplatin and gemcitabine in adults with solid tumors. *Clin. Cancer Res.* **2012**, *18*, 2344-2351.

- (28) Menear, K. A.; Adcock, C.; Boulter, R.; Cockcroft, X. L.; Copsey, L.; Cranston, A.; Dillon, K. J.; Drzewiecki, J.; Garman, S.; Gomez, S.; Javaid, H.; Kerrigan, F.; Knights, C.; Lau, A.; Loh, V. M., Jr.; Matthews, I. T.; Moore, S.; O'Connor, M. J.; Smith, G. C.; Martin, N. M. 4-[3-(4-cyclopropanecarbonylpiperazine-1-carbonyl)-4-fluorobenzyl]-2H-phthalazin-1-one: a novel bioavailable inhibitor of poly(ADP-ribose) polymerase-1. *J. Med. Chem.* **2008**, *51*, 6581-6591.
- (29) Jones, P.; Altamura, S.; Boueres, J.; Ferrigno, F.; Fonsi, M.; Giomini, C.; Lamartina, S.; Monteagudo, E.; Ontoria, J. M.; Orsale, M. V.; Palumbi, M. C.; Pesci, S.; Roscilli, G.; Scarpelli, R.; Schultz-Fademrecht, C.; Toniatti, C.; Rowley, M. Discovery of 2-{4-[(3*S*)-piperidin-3-yl]phenyl}-2H-indazole-7-carboxamide (MK-4827): a novel oral poly(ADP-ribose)polymerase (PARP) inhibitor efficacious in BRCA-1 and -2 mutant tumors. *J. Med. Chem.* **2009**, *52*, 7170-7185.
- (30) Thomas, H. D.; Calabrese, C. R.; Batey, M. A.; Canan, S.; Hostomsky, Z.; Kyle, S.; Maegley, K. A.; Newell, D. R.; Skalitzky, D.; Wang, L. Z.; Webber, S. E.; Curtin, N. J. Preclinical selection of a novel poly(ADP-ribose) polymerase inhibitor for clinical trial. *Mol. Cancer Ther.* **2007**, *6*, 945-956.
- (31) Wang, B.; Chu, D.; Feng, Y.; Shen, Y.; Aoyagi-Scharber, M.; Post, L. E. Discovery and characterization of (8*S*,9*R*)-5-fluoro-8-(4-fluorophenyl)-9-(1-methyl-1*H*-1,2,4-triazol-5-yl)-2,7,8,9-tetrahydro-3*H*-pyrido[4,3,2-*de*]phthalazin-3-one (BMN 673, Talazoparib), a novel, highly potent, and orally efficacious poly(ADP-ribose) polymerase-1/2 inhibitor, as an anticancer agent. *J. Med. Chem.* **2016**, *59*, 335-357.
- (32) Tang, Z.; Jiang, B.; Shi, Z.; Gong, W.; Liu, Y.; Wang, X.; Gao, Y.; Yu, F.; Zhou, C.; Luo, L.; Wei, M.; Wang, L. Abstract 1651: BGB-290, a novel PARP inhibitor with unique brain penetration ability, demonstrated strong synergism with temozolomide in subcutaneous and intracranial xenograft models. *Cancer Res.* **2015**, *75*, 1651-1651.
- (33) Plummer, E. R.; Dua, D.; Cresti, N.; Suder, A.; Drew, Y.; Stephens, P.; Foegh, M.; Knudsen, S.; McGonigle, S.; Ink, B.; Sarker, D. First-in-human phase 1 study of the PARP/tankyrase inhibitor 2X-121 (E7449) as monotherapy in patients with advanced solid tumors and validation of a novel drug response predictor (DRP) mRNA biomarker. *J. Clin. Oncol.* **2018**, *36*, 2505-2505.
- (34) McGonigle, S.; Chen, Z.; Wu, J.; Chang, P.; Kolber-Simonds, D.; Ackermann, K.; Twine, N. C.; Shie, J.-L.; Miu, J. T.; Huang, K.-C.; Moniz, G. A.; Nomoto, K. E7449: A dual inhibitor of PARP1/2 and tankyrase1/2 inhibits growth of DNA repair deficient tumors and antagonizes Wnt signaling. *Oncotarget* **2015**, *6*, 41307-41323.
- (35) Wang, L.; Yang, C.; Xie, C.; Jiang, J.; Gao, M.; Fu, L.; Li, Y.; Bao, X.; Fu, H.; Lou, L. Pharmacologic characterization of fluzoparib, a novel poly(ADP-ribose) polymerase inhibitor undergoing clinical trials. *Cancer Sci.* **2019**, *110*, 1064-1075.
- (36) He, J. X.; Wang, M.; Huan, X. J.; Chen, C. H.; Song, S. S.; Wang, Y. Q.; Liao, X. M.; Tan, C.; He, Q.; Tong, L. J.; Wang, Y. T.; Li, X. H.; Su, Y.; Shen, Y. Y.; Sun, Y. M.; Yang, X. Y.; Chen, Y.; Gao, Z. W.; Chen, X. Y.; Xiong, B.; Lu, X. L.; Ding, J.; Yang, C. H.; Miao, Z. H. Novel PARP1/2 inhibitor mefuparib hydrochloride elicits potent in vitro and in vivo anticancer activity, characteristic of high tissue distribution. *Oncotarget* **2017**, *8*, 4156-4168.
- (37) Velagapudi, Uday Kiran, et al. "Recent Development in the Discovery of PARP Inhibitors as Anticancer Agents: a Patent Update (2016-2020)." *Taylor & Francis*, 12 Mar. 2021, [www.tandfonline.com/doi/full/10.1080/13543776.2021.1886275](http://www.tandfonline.com/doi/full/10.1080/13543776.2021.1886275).



- (38) Zandarashvili, L.; Langelier, M. F.; Velagapudi, U. K.; Hancock, M. A.; Steffen, J. D.; Billur, R.; Hannan, Z. M.; Wicks, A. J.; Krastev, D. B.; Pettitt, S. J.; Lord, C. J.; Talele, T. T.; Pascal, J. M.; Black, B. E. Structural basis for allosteric PARP-1 retention on DNA breaks. *Science (New York, N.Y.)* **2020**, 368.
- (39) Velagapudi, U. K.; Langelier, M. F.; Delgado-Martin, C.; Diolaiti, M. E.; Bakker, S.; Ashworth, A.; Patel, B. A.; Shao, X.; Pascal, J. M.; Talele, T. T. Design and synthesis of poly(ADP-ribose) polymerase inhibitors: Impact of adenosine pocket-binding motif appendage to the 3-oxo-2,3-dihydrobenzofuran-7-carboxamide on potency and selectivity. *J. Med. Chem.* **2019**, 62, 5330-5357.
- (40) Talele, T. T. The "cyclopropyl fragment" is a versatile player that frequently appears in preclinical/clinical drug molecules. *J. Med. Chem.* **2016**, 59, 8712-8756.
- (41) Talele, T. T. Opportunities for tapping into three-dimensional chemical space through a quaternary carbon. *J. Med. Chem.* **2020**, 63, 13291-13315.
- (42) Patel, M. R.; Bhatt, A.; Steffen, J. D.; Chergui, A.; Murai, J.; Pommier, Y.; Pascal, J. M.; Trombetta, L. D.; Fronczek, F. R.; Talele, T. T. Discovery and structure-activity relationship of novel 2,3-dihydrobenzofuran-7-carboxamide and 2,3-dihydrobenzofuran-3(2H)-one-7-carboxamide derivatives as poly(ADP-ribose)polymerase-1 inhibitors. *J. Med. Chem.* **2014**, 57, 5579-5601.
- (43) Antolin, A.A., Ameratunga, M., Banerji, U. *et al.* The kinase polypharmacology landscape of clinical PARP inhibitors. *Sci Rep* **10**, 2585 (2020). <https://doi.org/10.1038/s41598-020-59074-4>
- (44) Gao, C.; Li, B.; Zhang, B.; Sun, Q.; Li, L.; Li, X.; Chen, C.; Tan, C.; Liu, H.; Jiang, Y. Synthesis and biological evaluation of benzimidazole acridine derivatives as potential DNA-binding and apoptosis-inducing agents. *Bioorg. Med. Chem.* **2015**, 23, 1800-1807.
- (45) Brady, P. B., W.; Dai, Y.; Doherty, G.; Gong, J.; Jantos, K.; Ji, C.; Judd, A.; Kunzer, A.; Mastracchio, A.; Risi, R.; Song, X.; Souers, A.; Sullivan, G.; Tao, Z. F.; Teske, J.; Wang, X.; Wendt, M.; Yu, Y.; Zhu, G.; Penning, T.; Lai, C.; Kling, A.; ; Pohlki, F. P., D.; Guillier, F. Macrocyclic MCL-1 inhibitors and methods of use. W. O. Patent 035,914, Feb 21, 2019.
- (46) Dunetz, J. R.; Magano, J.; Weisenburger, G. A. Large-scale applications of amide coupling reagents for the synthesis of pharmaceuticals. *Org. Process Res. Dev.* **2016**, 20, 140-177.
- (47) Clayden, Jonathan (2005). *Organic chemistry* (Reprinted(with corrections) ed.). Oxford [u.a.]: Oxford Univ. Press. pp. 296. ISBN 978-0-19-850346-0
- (48) Shao X, Pak S, Velagapudi UK, Gobbooru S, Kommaraju SS, Low WK, Subramaniam G, Pathak SK, Talele TT. Synthesis of 2,3-dihydrobenzo[b][1,4]dioxine-5-carboxamide and 3-oxo-3,4-dihydrobenzo[b][1,4]oxazine-8-carboxamide derivatives as PARP1 inhibitors. *Bioorg Chem.* 2020 Sep;102:104075.

## Vita

Name	<i>Griffin Coate</i>
Baccalaureate Degree	<i>Bachelor of Science, University of Connecticut, Storrs Major: Structural Biology/Biophysics</i>
Date Graduated	<i>May, 2019</i>